Impact of the photo cathode laser temporal modulation onto longitudinal phase space

Burnaev Evgeny
Moscow Institute of Physics and Technology (State University)
141700, Moscow Region, Dolgoprudniy town, Institutskiy Side Street, 9.
Email: drazil@list.ru

The main challenge of the Photo Injector Test Facility at DESY Zeuthen (PITZ) is optimizing an electron source for Free Electron Lasers and future colliders. One of the problems is that a high-brightness electron beam with a small amount of longitudinal density modulation can create additional beam energy modulation due to collective fields - Longitudinal Space Charge (LSC), Coherent Synchrotron Radiation (CSR), geometrical wakefields, that can be converted to additional density and energy modulations in a subsequent magnetic bunch compressor. This process distorts longitudinal phase space (LPS) of the electron bunch and is usually accompanied by the emittance growth. To all appearance, initial density modulations are produced by non-ideal laser temporal intensity distribution. Moreover, during experiments at DESY - PITZ it was observed, that these initial modulations can be smeared out with and increase of the electron bunch charge. Therefore, investigations of impact of the photo cathode laser temporally modulated intensity distribution onto LPS is needed, especially, dependence of the smearing effect on the bunch charge, modulation depth and frequency should be studied.

The method of simulating temporally modulated intensity distribution of laser pulse is discussed. The concept of the local skeleton of non-modulated LPS is introduced and the method of "straightening" of modulated LPS for further analysis is explained. The measures of similarity, based on local skeleton and longitudinal emittance are suggested. The analyses of modulated and non-modulated LPSs are included. The dependence of the introduced measures of similarity on the electron beam charge and the number of crests of the initial modulated intensity distribution are discussed. Simulated momentum distributions of modulated LPS after the booster cavity are included and compared with experimental results. Qualitative explanations of the observed phenomena are suggested, main results are summarized and proposals for future research are given. Additionally, during simulations with ASTRA [42] some artificial numerical "noisy" spikes were observed. The reasons of their appearance are also discussed and their spectral content is investigated using Fourier and wavelet spectra.

1 Introduction

1.1 General information

During the past decade a growing demand for a new generation of light sources has initiated research and development of high-gain free-electron lasers (FEL) for production of photons with laser properties [1], [2]. New light sources are required, having unprecedented brightness along with flexible temporal properties of radiation from the extreme ultraviolet

to x-ray wavelength range [1-4]. This requirements place serious constraints on the allowable quality of the accelerators-FEL drivers and used “active medium”. This quality can’t be achieved by usual circular accelerators due to huge energy loss because of synchrotron radiation. Since the energy loss increases proportionally with the electron energy to the power of four, energy of a few tens GeV is an upper limit for circular accelerator. Therefore, the electron bunch has to be accelerated on a straight trajectory in a **lin**ear **ac**celerator (linac) to reach energy more than 100 GeV, necessary for reaching desired electron peak current, capable of inducing the collective FEL instability. Also, such linac can be used as a superconducting linear collider to observe collisions of electrons and positrons with energies up to the order of TeV. However, for linac it is essential that the electron beam has small cross section and angular divergence (this means a small normalized emittance ~ 1 μm) and a very high peak current (approximately a few kA) in comparison with the circular accelerator. Moreover, small emittance will allow the reduction of the number of undulators.

PITZ (The **P**hoto **I**njector **T**est Facility at DESY **Z**euthen) is a test facility at DESY Zeuthen for research and development on the laser driven electron sources [6], [21]. The main challenge is to produce an intensive electron beam with a very small transverse emittance and rather small longitudinal emittance. The operation includes a continuous conditioning, characterization of the gun, test of new components and optimization. The TESLA Test Facility (TTF) working as VUV-FEL at DESY Hamburg is already running with a gun characterized at PITZ, but to fulfill the high requirements for the European X-ray-free-electron-laser (XFEL) an extension of the PITZ facility and its research program is necessary.

1.2 Overview of PITZ

1.2.1 PITZ set-up

The general setup of PITZ is schematically shown in figure 1.1. The facility consists of a cathode laser system, a RF-system and the acceleration elements with several subcomponents. The latter is divided into three sections: the cathode section, the gun section, the booster cavity and the diagnostic section.

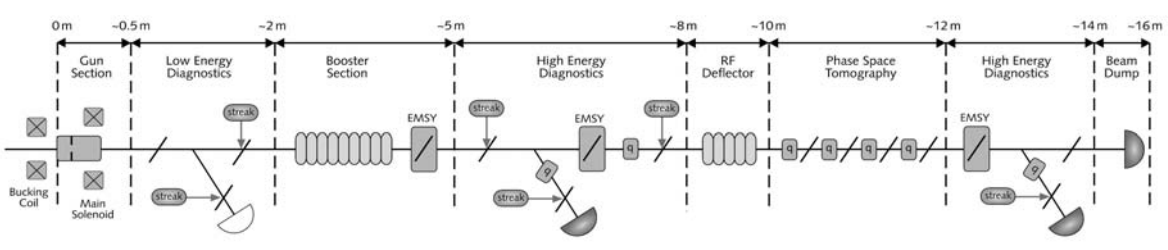

Figure 1.1: Schematic diagram of the PITZ set-up.

The gun section is consists of a 1.5 cell copper cavity with a coaxial RF coupler and solenoids for focusing the beam transversally and compensation of space charge induced emittance growth. The schematic diagram of the RF gun section is depicted in figure 1.2.

Further magnets are placed in the diagnostics section besides elements to analyze the beam properties.

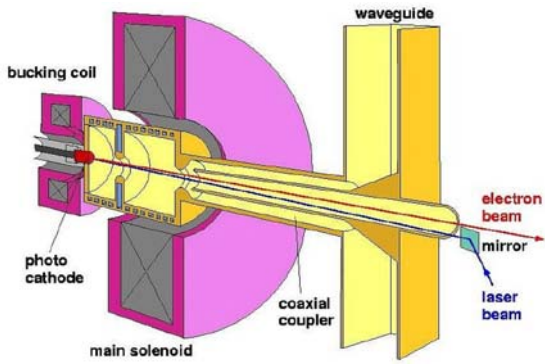

Figure 1.2: Schematic view of the RF gun.

A pulsed laser beam (wavelength $\approx 262\,nm$, pulse energy $\approx 22\,\mu J$) hits the cathode and due to the photoelectric effect electron bunches with a similar time structure are produced. For a standard operation, a Cs2Te cathode is used due to its quantum efficiency (up to 10%) and relative long life time [5]. The electrons, leaving the cathode, are immediately accelerated to energy of several MeV due to an electromagnetic standing wave with frequency 1.3 GHz inside the cavity to minimize the beam quality degradation due to the space charge forces. The RF gun cavity is fed by a klystron with 10 MW peak power. High maximum cavity field amplitude provides high acceleration gradient and therefore higher beam energy. This reduces the increasing of the beam emittance due to a space charge. A waveguide leads the RF field to the coaxial coupler which is connected with the cavity. The bucking coil compensates the magnetic field at the cathode. Optimization of the beam properties is mainly done to lower its emittance. The other parts of PITZ setup are extensively discussed in [7], [8], therefore we will concentrate on the discussion of the laser system and its properties, because it is necessary for understanding the motivations of this research.

1.2.2 The laser system and its properties.

The laser system at PITZ was developed at the Max Born Institute (MBI) and further development is ongoing. The schematic layout of the laser system is shown in figure 1.3 [9], [10]. The oscillator and the preamplifiers of the laser are laser diode pumped. To produce the electron bunches in synchronization with the accelerating RF-field, the laser oscillator is synchronized with the RF-frequency of 1.3 GHz by the means of an electro-optic modulator (EOM).

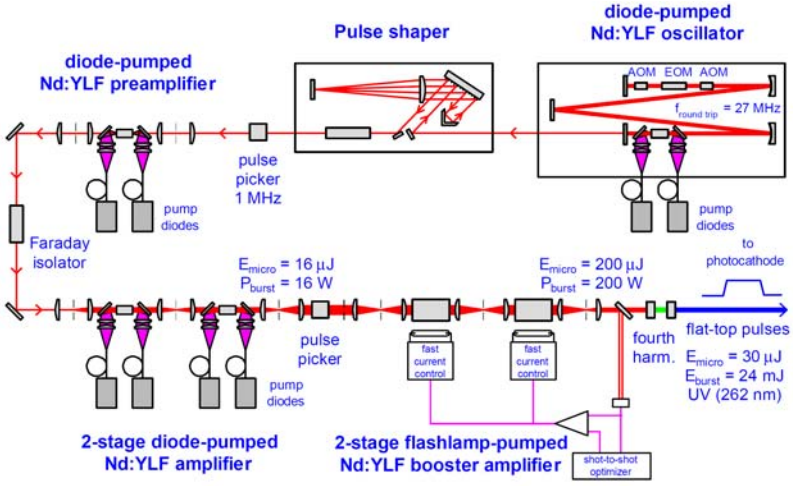

Figure 1.3: Layout of the PITZ laser system.

The oscillator produces laser pulses of some picoseconds with a temporal Gaussian shape. The following pulse shaper (by spectral masking) varies the temporal shape of the micro pulses to the flat-top shape. The laser should produce a radially and longitudinally uniform photon density on the photocathode. This type of distribution is preferred for the reduced impact on the beam emittance, since the transverse space charge forces within the bunch remains linear [12]. Pulse shaping, method for generation of the micropulses with desired shape, is based on spatial splitting of the individual spectral components of the laser pulse by means of gratings. Subsequently, the spectrum in the Fourier plane is modified with the aid of masks and transmission filters. This procedure results in micropulses of the desired shape after recombination of the individual spectral components. The pulse shaper is followed by diode pumped preamplifiers and two flash-lamp pumped booster amplifiers, which increase the energy of the IR pulse to 200 μJ (recently the laser has been upgraded, and now it is full diode-pumped based system). Neodymium doped Yttrium Lithium Fluoride (Nd:YLF) is used as laser material, which produces laser light at a wavelength of 1047 nm. The energy of photons with this wavelength is not sufficient to produce electrons in Cs2Te. For a sufficient quantum efficiency ultraviolet light is required. Two non-linear optical crystals transform the wavelength to the fourth harmonic. The Cs2Te cathodes have quantum efficiency at a wavelength of 262 nm up to 10% [5]. The UV micropulses have energy of 24 μJ. The laser system produces a pulse train with a variable length up to 800 μs. The pulse train consists of pulses with a pulse length of about 20 ps FWHM. In future the rising time should be minimized from around 8 ps to 2 ps to decrease the beam emittance. The laser light is transported by some mirrors and lenses onto the cathode. In the transport line a diaphragm is situated to change the transversal beam size.

The temporal and transverse properties of the individual laser pulses on the photo-cathode play a major role in obtaining a good electron beam quality. Therefore, those parameters are regularly monitored using a streak camera for the temporal laser profile and a CCD camera at a position equivalent to the photo-cathode location (virtual cathode) for the transverse laser shape.

1.3 Motivations of the research

To reduce transverse emittance the bunch length generated in the gun should be long, but a long bunch increases the longitudinal emittance and due to the cosine like RF field the longitudinal emittance in the acceleration section grows. A short bunch length would increase the transverse emittance due to space charge forces. Therefore, a relatively long bunch (FWHM=20 ps) has to be used initially. When energy higher than 100 MeV is reached space charge forces become weaker and the longitudinal distribution can be reduced by bunch compressor. To reach an optimum bunch compression in the first chicane the longitudinal phase space has to be defined as follows: the momentum of the electrons in the head of the bunch has to be smaller than the one of the electrons in the tail. The phase of the accelerator before the bunch compressor can be chosen in such a way that this condition is fulfilled.

However this method also has disadvantages, in particular, instabilities can occur. Further some experimental evidences of these instabilities will be given and some theoretical models considered.

1.3.1 Experimental observations

Several years ago two FEL facilities reported observations of a new complicated phenomenon. At the commissioning stage of Deep Ultraviolet FEL (DUV-FEL at NSLS, BNL) and TESLA Test Facility (TTF) FEL (DESY), strong modulations of the electron bunch energy spectra was observed [13], [14]. During measurements of the bunch length using the so-called zero-phasing method [15] the energy spectra of the compressed bunch exhibited spiky structure with subpicosecond separation. In figure 1.4 there are examples of the appearance of the microbunching within a single electron bunch with increase of compression [13]. The peaks in the time distribution of this example are just 50 fs FWHM wide, and the spacing between peaks is 140 fs. Similar results from experimental observations and numerical simulations are also presented in [16], [17], [18], [19]. In these works it was also was observed, that the energy distribution of the beam, when fully longitudinally compressed, breaks up into several peaks.

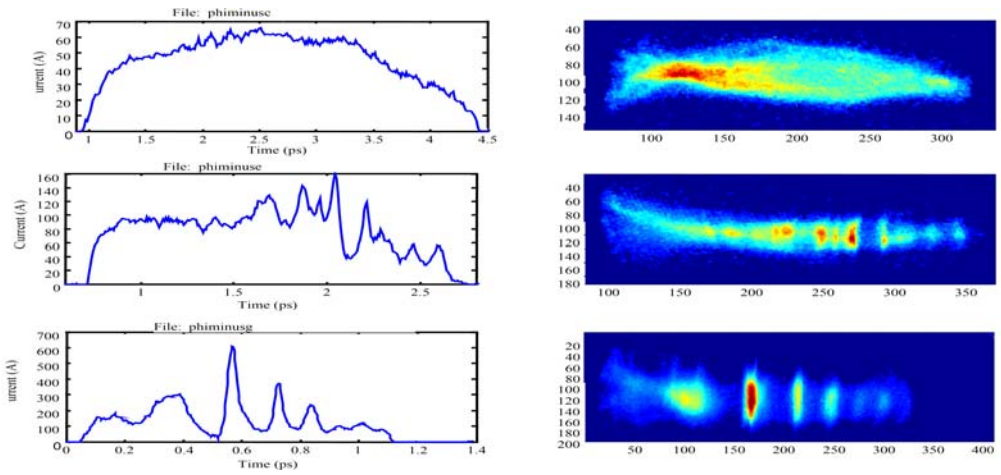

Figure 1.4: No compression (top), mild compression (middle; microbunching begins to appear), strong compression (bottom; microbunching apparent), Q=250 pC [13].

1.3.2 Theoretical models of instability

The most probable explanation of the observed phenomenon is that a high-brightness electron beam with a small amount of longitudinal density modulations (with frequency higher than typical inverse pulse duration) can create additional beam energy modulations due to collective fields (Coherent Synchrotron Radiation, geometrical wakefields, Longitudinal Space Charge field) [22-36], [17], [37], [38].

In case of CSR or geometrical wakefields energy modulations can be created if there is a magnetic bunch compressor downstream. It is used to compress the electron bunch from several picoseconds duration to less than 1 ps duration and at the same time compressor amplifies the peak electron beam current from tens to hundreds of amperes. As the electron bunch becomes shorter, the relatively weak incoherent radiation emitted as either synchrotron light in the magnetic bends, wakefields in the vacuum chamber, or transition radiation as it traverses different materials can become coherent at wavelength comparable to features on the electron bunch. E.g., the mechanism of CSR induced energy modulations can be described in the following way. Electron on its curved trajectory in bend magnets emits radiation, which again moves forward in the beam, because the radiation propagates faster, and in a straight line. The radiation field and electron cross at an angle (typically much lager than in an FEL undulator) yielding a longitudinal electric field component, which changes the electron energy. The light intensity is then enhanced by the number of electrons, a factor of 10^9, raising peak power to the level of hundreds of megawatts. The strong radiation may interact further with electrons, causing modulations in their energy or time distributions. Such distortions may be very large for short-wavelength FELs when multistage bunch compression is incorporated. Moreover, the CSR can be strongly enhanced due to local charge concentration, as pointed out in [20], for example due to longitudinal phase space curvature. Theoretical models, simulation results and calculations of gain in amplitude for density/energy modulations for CSR and wakefields were investigated in [22-36].

The model of the LSC field induced energy modulations is based on the longitudinal space-charge effect, which drives small nonuniformities in the longitudinal bunch density into energy modulation along the bunch [17], [37], [38]. Small density clusters in the electron bunch create longitudinal space-charge field that accelerates particles at the head of the cluster and decelerates particles at the tail. This initiate space-charge oscillations in the bunch as it travels along the accelerator (e.g., booster cavity, which is necessary to compensate space charge forces). As a result, the initial density modulations at the injector end may be reduced by a factor of a few, while noticeable energy modulations can be accumulated in the injector. That’s why the longitudinal phase-space distribution of the electron bunch at the end of the accelerator is strongly distorted. This effect is emphasized in the high-peak current regime required for achieving high gain in a single-pass FEL.

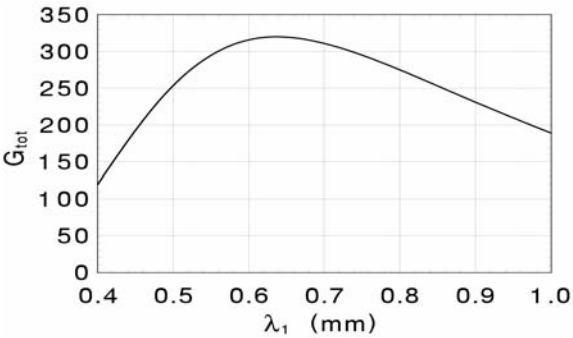

Figure 1.5: Total gain versus initial modulation wavelength [38].

Imagine that after the accelerator there is a magnetic bunch compressor. Since compressor (usually a magnetic chicane) introduces path length dependence on energy, the induced energy modulations is then converted to additional density modulations that can be much larger than the initial density modulations. This amplification process is accompanied by a growth of energy modulations and a possible growth of emittance if significant energy modulations are induced in a dispersive region such as the chicane. In other words, the system can be treated as a high-gain klystron-like amplifier. The general tendency is that higher modulations frequencies (to some extent) are going to get amplified stronger so that they may become much better pronounced in comparison with the case of undisturbed compression in chicane. Thus, the instability can be harmful to the FEL performance, which depends critically on the high quality of the electron bunch.

It was estimated, that the LSC field can be the main effect, driving the instability [38]. In this report authors supposed that initial energy spread is Gaussian with some modulations. They estimated the total gain in the amplitude of the density modulations that can be achieved due to LSC effect in TESLA Test Facility Free Electron Laser with two bunch compressors. In figure 1.5 the dependence of the total gain on the initial density modulations wavelength is depicted [38]. It can be seen, that the length, where the maximum gain is achieved, is comparable to features on the electron bunch. It should be noticed that similar estimation of gain due to CSR was lower in two orders [22-36].

Possible solutions for suppressing these instabilities have been proposed and studied [38-39], [41]. E.g., in [39] it is proposed to use a superconducting wiggler or the resonant laser-electron interaction in an undulator (a laser heater) to introduce additional energy spread that can smear out modulations.

1.3.3 Reasons for distortions of Longitudinal Phase Space (LPS) in PITZ

It is worth to notice, that all of the mentioned theoretical works considered electron bunch (usually with near relativistic energies) with some density modulations before the entrance to the bunch compressor or linac. However, none of the mentioned works consider the mechanism of appearance of density modulations, how these modulations can change immediately after RF gun without any bunch compression and what influence have the main parameters of the electron bunch on these modulations.

The initial density modulations are most likely caused by the intensity fluctuations on the drive laser that produces the electron beam from the photocathode. The photocathode laser is assumed to have a flat-top temporal profile with 20 ps FWHM and 2

ps rise/fall time. However, from figure 1.6 it is obvious that the temporal profiles do not have the desired flat-top distribution but they are more close to a truncated Gaussian distribution with some modulations at the top. These modulations are at time scales of about 5-10 ps. It should be noted, that the percentage of modulations, that is written in the figure 1.5 is equal to the ratio of the difference of areas of modulated distribution and flat-top fit to the square of flat-top fit. In fact it isn't difficult to evaluate that in accord with plots, the modulations are approximately 10%-40% of the maximum level of the corresponding flat-top fit.

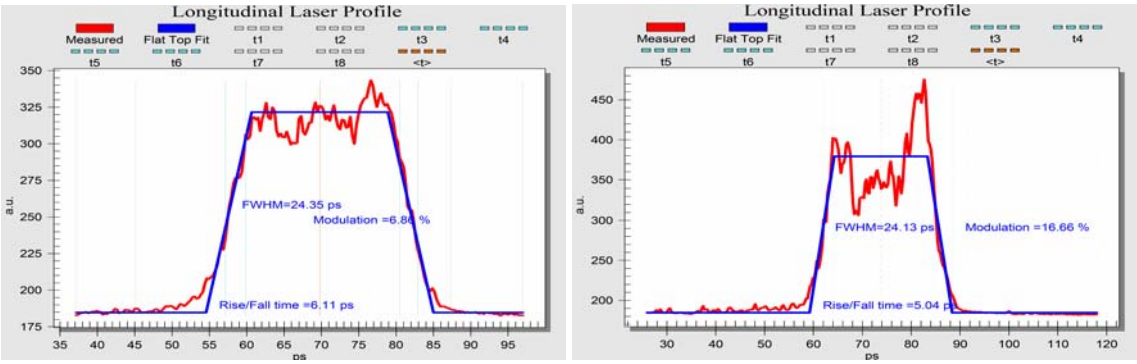

Figure 1.6: Examples of real temporal laser profile with flat-top fit (PITZ - DESY), measured with streak camera.

In reality modulations of the laser temporal distribution can be bigger, because the resolution of the streak camera depends on the following effects [40]: jitter of the laser and the RF-field, brightness of Cherenkov light, value of photon density; also streak camera slit width smears the signal, and so on. In the first example three crests can be easily distinguished; to all appearance there are also three crests in the second example but two of them merged and can't be recognized easily. These distortions of temporal laser energy distribution can lead to significant initial density modulations of an electron bunch.

Also, during experiments in DESY, PITZ it was observed [11] that subsequent distortions of the LPS immediately after RF gun significantly depend on bunch charge; moreover, these distortions could be smeared out with an increase of bunch charge. So, maybe it is possible to find out such value of the bunch charge, which, on the one hand, will be enough for experiments and on the other hand will provide the highest smearing effect. For the above reasons the investigation of the impact of the photo cathode laser temporally modulated intensity distribution onto LPS is needed, especially, dependence of the smearing effect on the bunch charge, modulation depth and frequency should be studied.

In section 2 the method of simulating temporally modulated intensity distribution of laser pulse is discussed. The notion of the local skeleton of non-modulated LPS is introduced and the method of "straightening" of modulated LPS for further analysis is explained. The concepts of similarity, based on local skeleton and longitudinal emittance are suggested. The analyses of modulated and non-modulated LPSs are included. The dependence of the introduced measures of similarity on the electron beam charge and the number of crests of the initial modulated intensity distribution are discussed. Simulated momentum distributions of modulated LPS after the booster cavity are included and compared with plots of real experimental momentum distributions. In section 3 some

explanations of the observed phenomena are suggested, main results are listed, directions for future research are given. In appendix A content of ASTRA [42] input files generator.in and rfgun.in is included. In appendix B plots of modulated and non-modulated LPSs are depicted. Additionally, during simulations with ASTRA some artificial numerical “noisy” spikes were observed. The reasons of their appearance are also discussed and their spectral content is investigated in appendix C using Fourier and wavelet spectra.

2 ASTRA simulations of modulated LPS

The macroparticle code ASTRA, which incorporates a space charge algorithm on a rotational symmetric mesh, has been used for simulations of modulated longitudinal phase space. Typical parameters, used during simulations, are listed in the Appendix A.

2.1 Generation of a modulated LPS

Obviously, for generation of modulated longitudinal phase space we have to introduce some modulations to the initial temporal intensity distribution of the laser beam. The following technique was proposed. Let’s denote N - number of crests, $depth\ (0 < depth < 1)$ - an amplitude of introduced modulations, $T = 1.2 \cdot FWHM$, where FWHM - Full Width Half of Maximum of temporal distribution of laser beam. First of all, using usual generator.exe initial intensity distribution was generated. Then, using **clock** column of output file from generator.exe, histogram (temporal intensity distribution) was calculated. In figure 2.1 a typical example is depicted (in blue). Starting with the points, which abscissa lie in the interval $\left[-T/2, T/2\right]$, the ordinates of modulated histogram (modulated intensity distribution) are calculated using the following formula:

$$\tilde{y}(t) = y(t) \cdot \left(1 + depth \cdot \sin\left[\frac{\left(t + T/2\right) \cdot \pi \cdot \left(2 \cdot N - 1\right)}{T}\right]\right),$$

where (t, y) - coordinates of a point of non-modulated histogram and $(t, \tilde{y})$ - coordinates of a point of modulated histogram. The result of this transformation is depicted in figure 2.1 (in red, $depth = 0.5$). Then, to introduce modulations to the electron bunch, charge of each particle from column **macro charge** with **clock** parameter t was transformed using the following formula:

$$\tilde{q}(t) = q(t) \cdot \frac{hm(t)}{h(t)},$$

where $q(t)$ - charge of “non-modulated” particle, $\tilde{q}(t)$ - charge of “modulated” particle, $h(t)$ and $hm(t)$ are depicted in figure 2.1. To get values $h(t)$ and $hm(t)$ interpolation of non-modulated and modulated histograms with cubic splines was used. This method promotes to avoid sharp features in the modulated intensity distribution (it is very important, because in case of sharp features LPS, generated from this initial distribution, will have artificial thickening). At the beginning of the present research another method for generation of modulated density distribution of laser beam was considered. However, produced modulated density distribution introduced some noise to LPS (Appendix C). The

present method doesn't break quasi-random coordinate distribution of particles in contrasts to previous one. In figure 2.2 there is an example of modulated density with three crests (N=3).

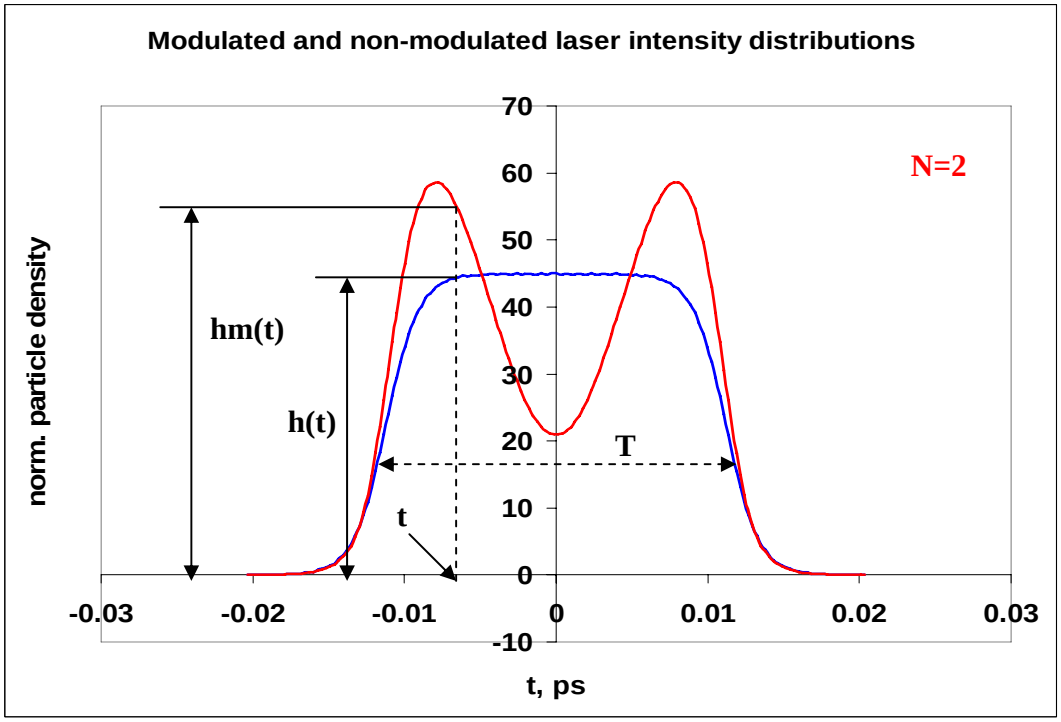

Figure 2.1: Generation of modulated longitudinal distribution

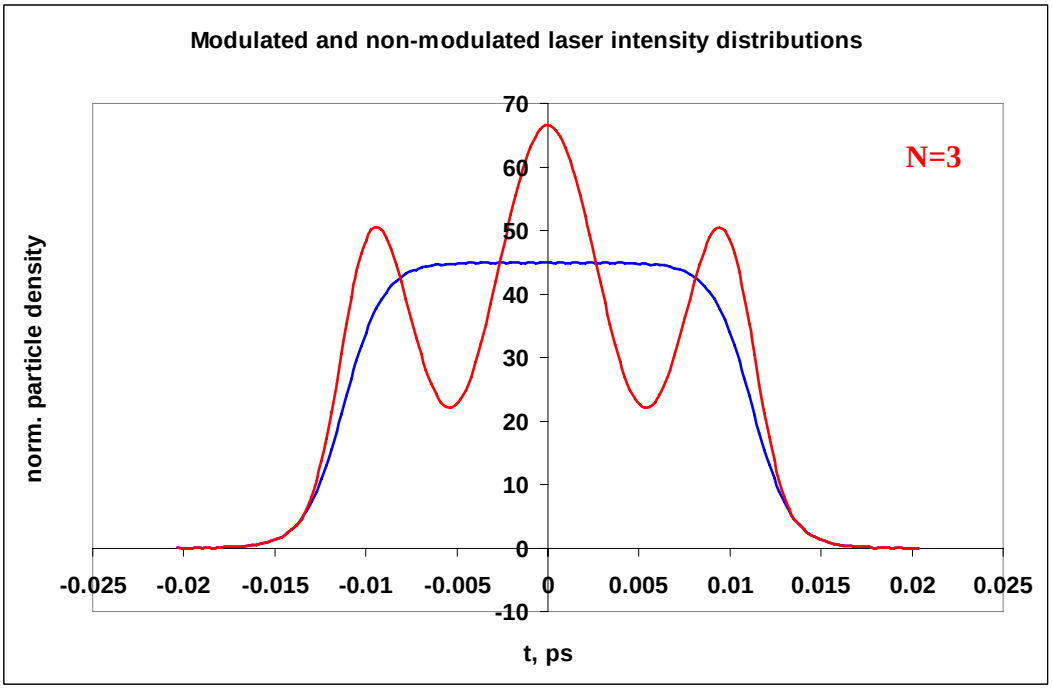

Figure 2.2: Example of modulated and non-modulated laser intensity distributions

In figures 2.3, 2.4, 2.5, 2.6, 2.7 plots of non-modulated (left) and modulated (right) LPS in contour lines, overlapped modulated (red) and non-modulated (blue) LPS, longitudinal distribution and momentum distribution of modulated (red) and non-modulated (blue) LPS are depicted for charges of electron bunch, equal 0.05, 0.15, 0.3, 0.7 and 1.0 nC correspondingly. In this simulations modulated initial intensity distribution of laser beam has two crests (N=2) with $depth = 0.5$, ZSTOP=3.6. It should be noted, that graphs of LPS in contour lines differs from graph of overlapped LPSs, because of two reasons. First, graphs in contour lines show the head of the bunch on the left (at negative times) and the tail on the right, whereas all other plots imply the opposite disposition. Second, for depiction of plots in contour lines the head and tail of the bunch were cut off, that is particles with longitudinal momentum bigger, then some threshold, were not included. It can be seen that with increase of charge two crests of modulated longitudinal distribution smear out and it becomes like non-modulated longitudinal distribution. Momentum distribution also has two crests which with the increase of the charge smear out. However, non-modulated momentum distribution of for case of charge, equals to 1 nC, is more degraded. From plots with overlapped modulated and non-modulated LPSs it can be seen that modulations become less prominent with increase of the charge. Also, two separate maxima (observable in contour lines) of modulated LPS merge with the increase of the charge. All these observations indirectly confirm hypothesis that modulations can be smeared out with the increase of the electron charge of the beam. Examples of such plots but for other number of crests (N=3) are presented in Appendix B. The same observations about their features as above can be made. However, some measures of similarity should be introduced and their dependence on the charge should be investigated for better understanding of the phenomenon under consideration.

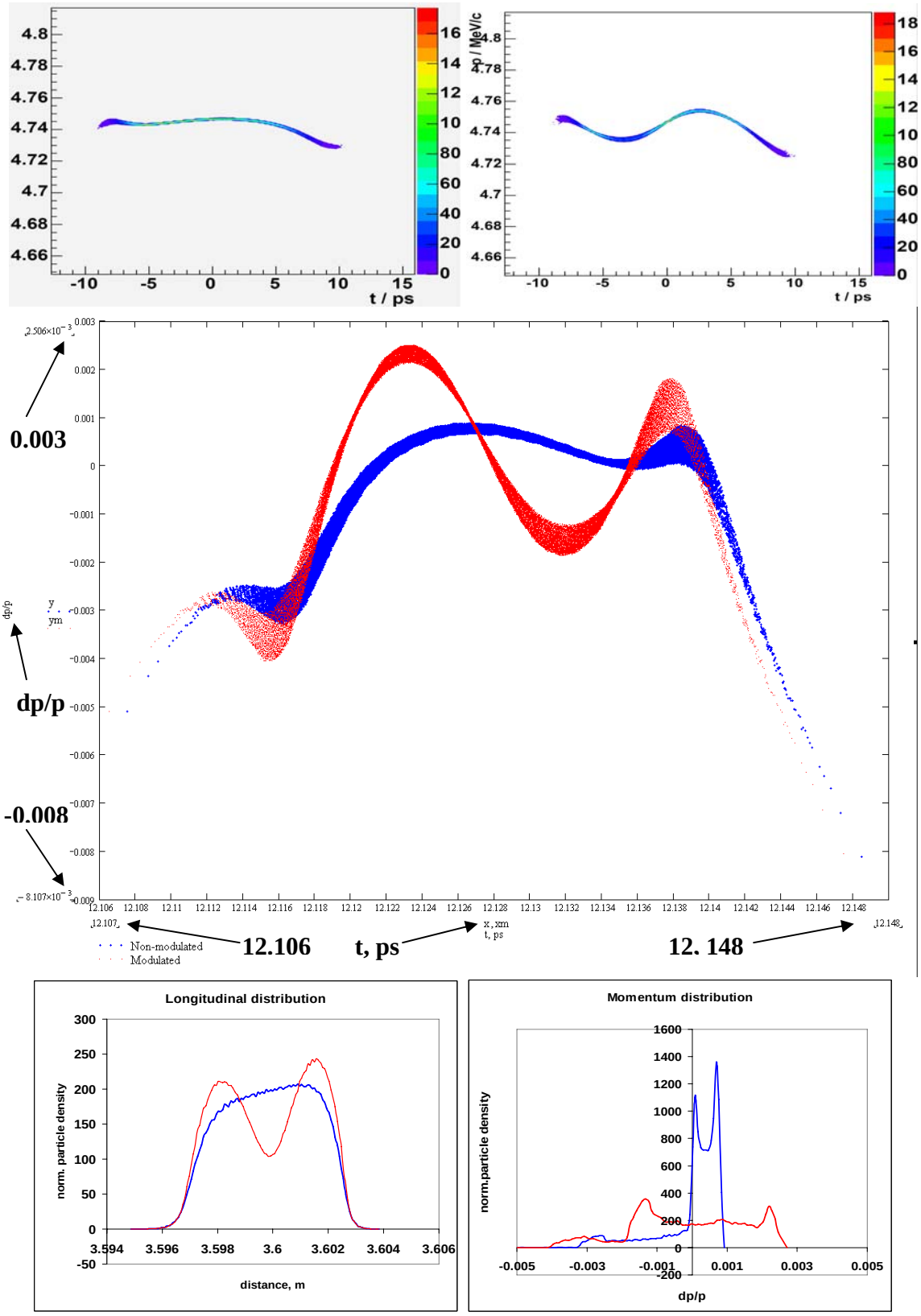

Figure 2.3: Q=0.05 nC (details in text).

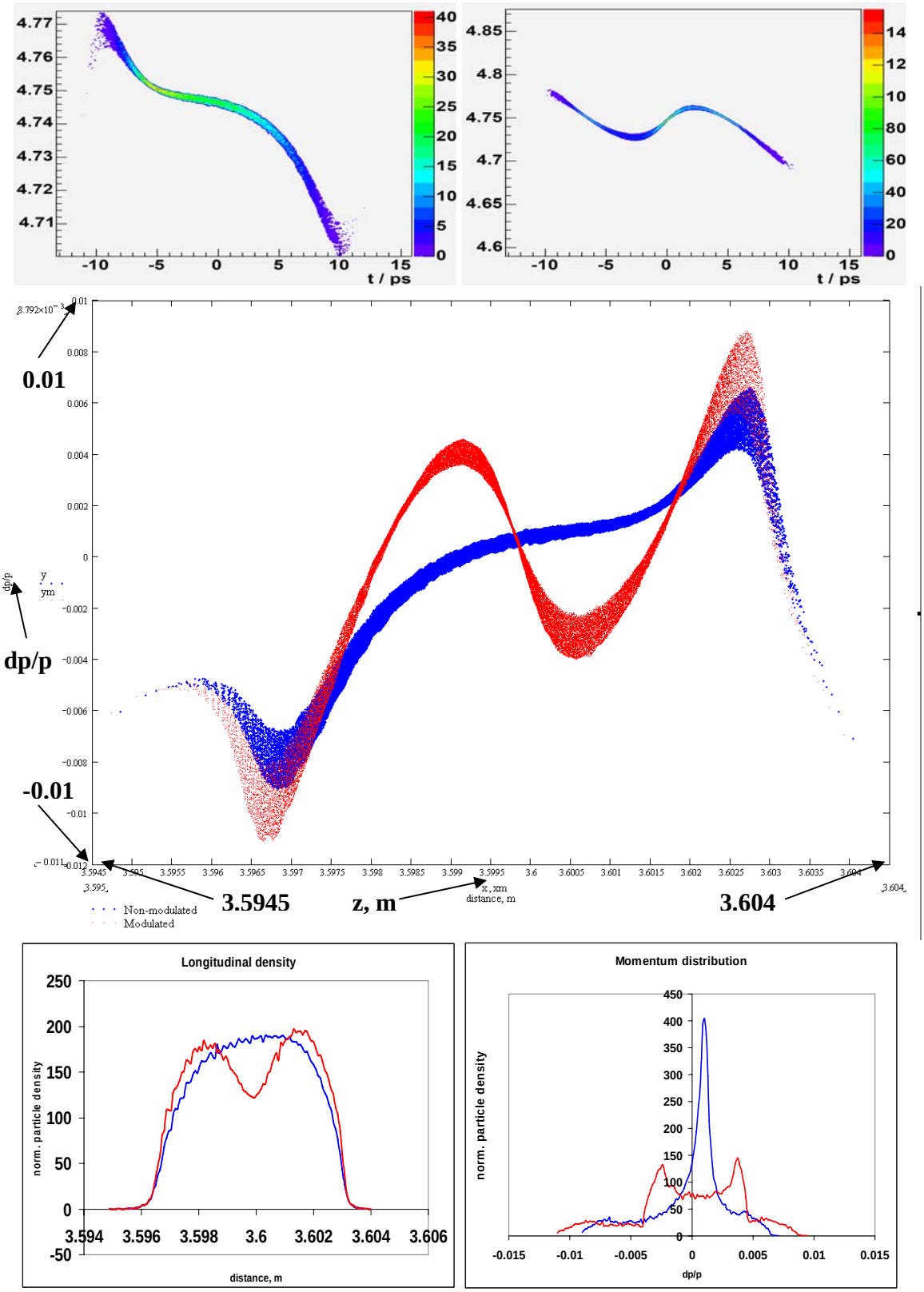

Figure 2.4: Q=0.15 nC (details in text).

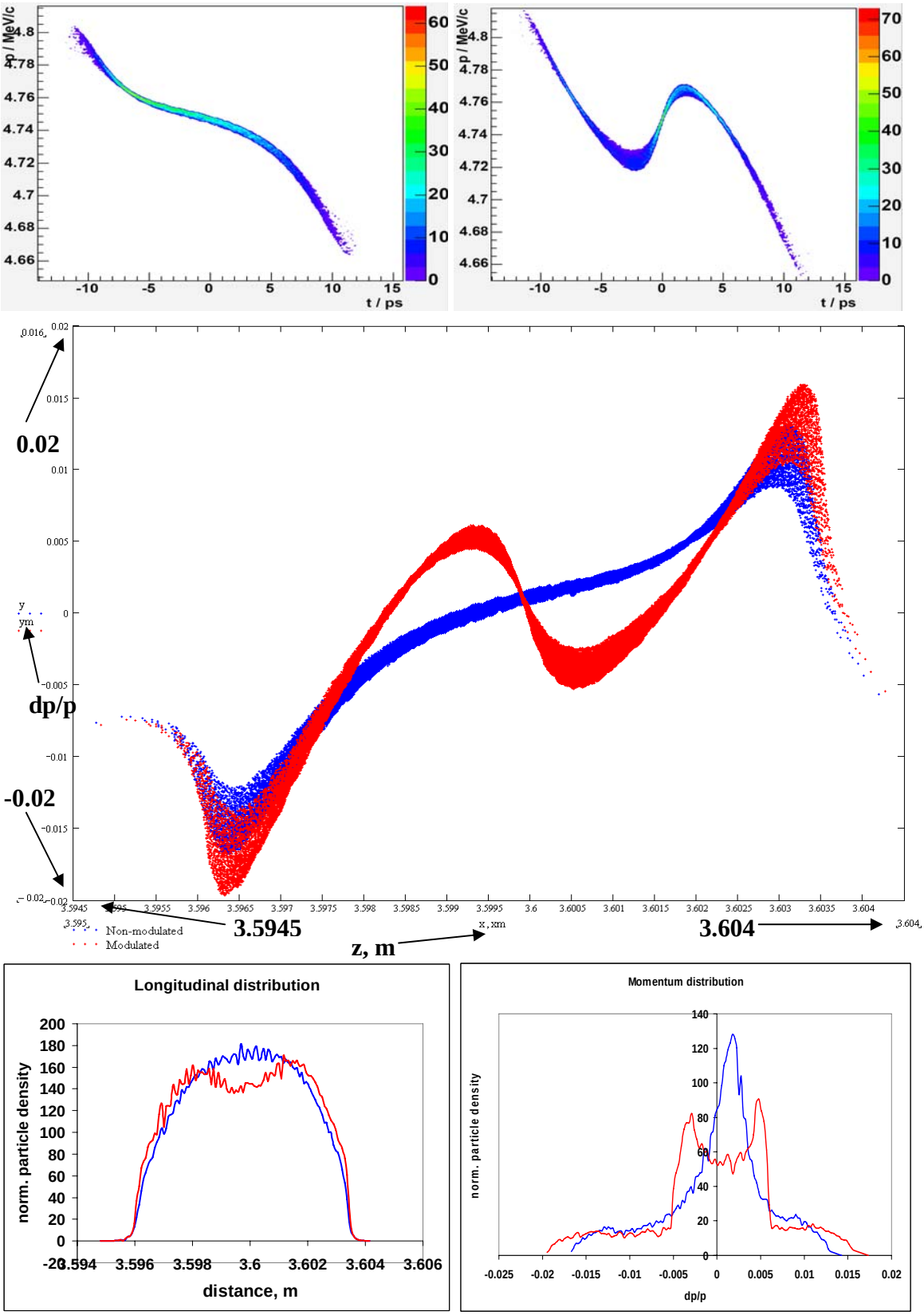

Figure 2.5: Q=0.3 nC (details in text).

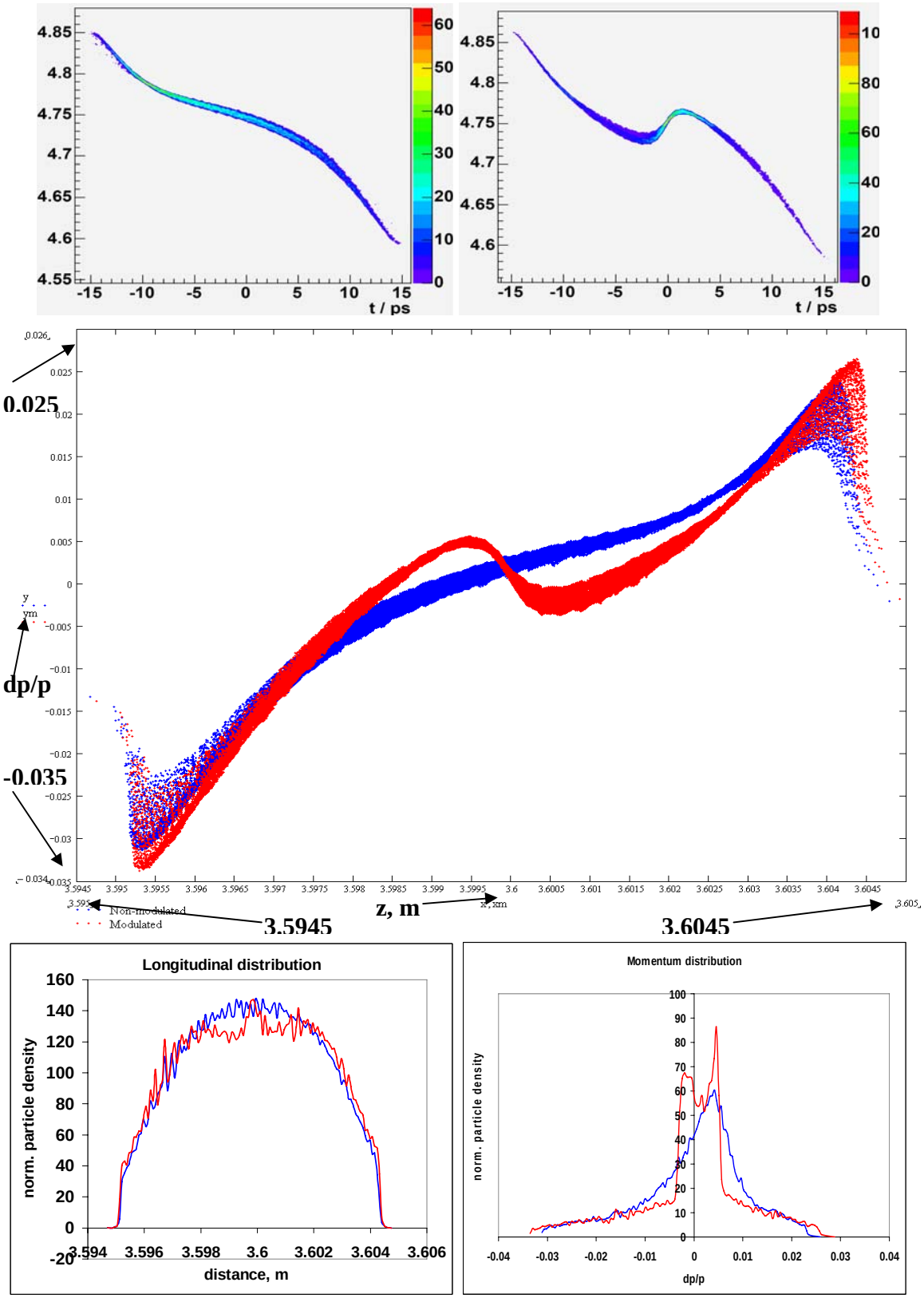

Figure 2.6: Q=0.7 nC (details in text).

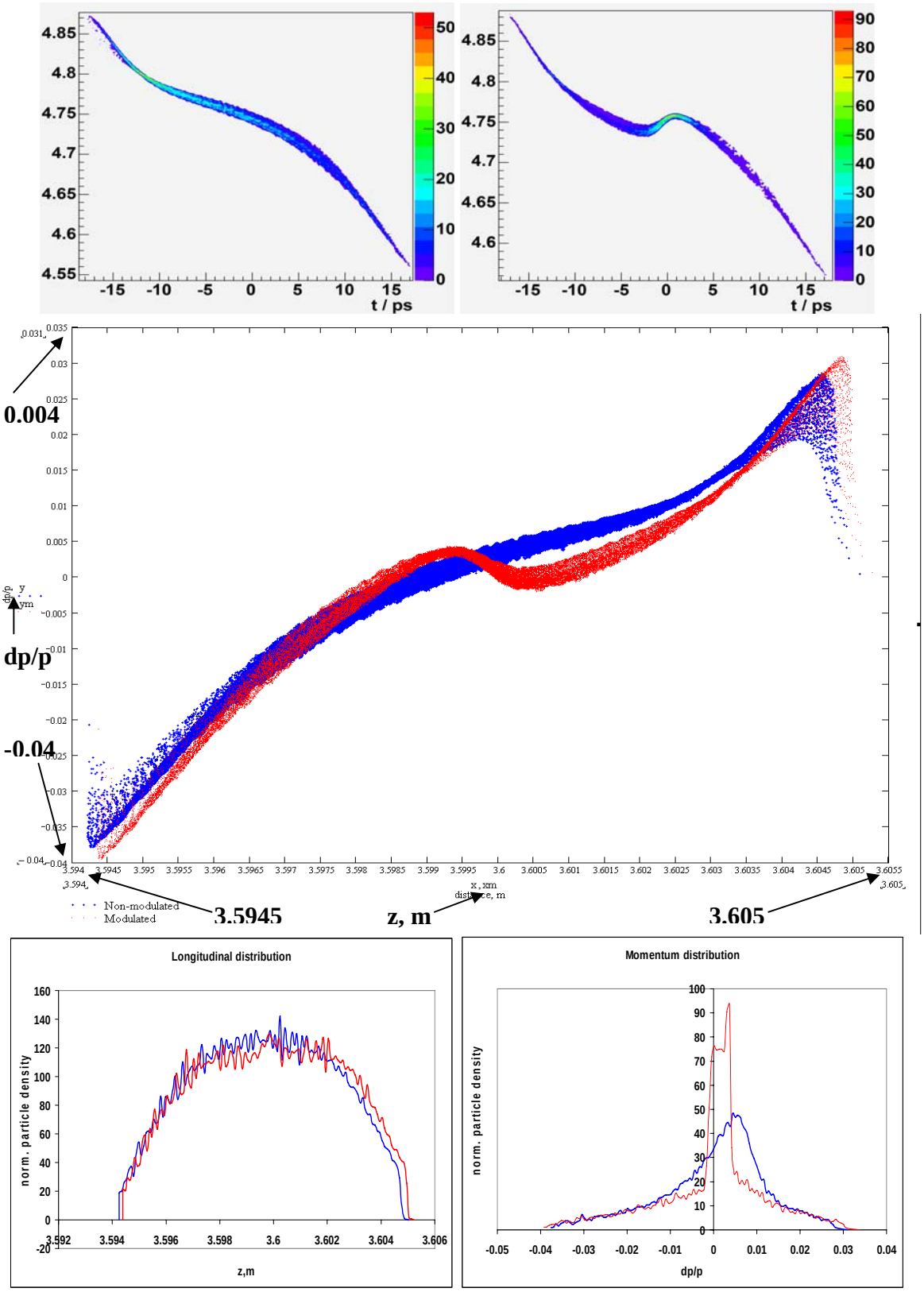

Figure 2.7: Q=1.0 nC (details in text).

2.2 Measures of similarity

2.2.1 Skeleton based measure of similarity

It can be seen from figures 2.3, 2.4, 2.5, 2.6 and 2.7 that even non-modulated LPS is highly nonlinear. So, for better analysis of modulations the process of "straightening" of LPS was proposed. First of all, a skeleton of non-modulated LPS and its coordinates w.r.t. this skeleton should be obtained. In figure 2.8 this process is depicted. First, non-modulated LPS curve is cut into slices (usually it was 200 slices), for every slice coordinates of central point is obtained (mean abscissa and ordinate of all points in the slice). Line, connected these central points, is called skeleton of the LPS. Then, in each slice its own local non-Euclid coordinate system is introduced – ordinate axes are all different for different slices (Y1, Y2 and so on in figure 2.8), but abscissa axe is the same (abscissa coordinate is approximately equal to the mean length of the curve). Non-Euclid coordinate system was used because in such case the ordinate keeps its physical meaning – momentum distribution. In figure 2.9 the skeleton (in black) of the non-modulated LPS for Q=0.01 nC is depicted. There is also modulated LPS in this figure. It is obvious, that plot of modulated LPS in such local coordinate system w.r.t. non-modulated LPS will underline modulations. Modulated and non-modulated LPS in such local coordinate system of non-modulated LPS is called straightened LPS. Then, again skeletons of both straightened LPS is obtained as it was explained earlier, and using these skeletons, measure of similarity is introduced. The only difference with the above skeleton of non-modulated LPS is that abscissas of these skeletons were fixed – they were the abscissas of the center of slices. Usually, also 200 slices were used to produce these skeletons. In figure 2.10 straightened LPS and their skeletons are depicted for Q=0.01 nC. Skeleton of modulated LPS perfectly detects introduced modulations. In figure 2.11 there are examples of skeletons of straightened LPSs for Q=1.0 nC (right) and Q=1.5 nC (left).

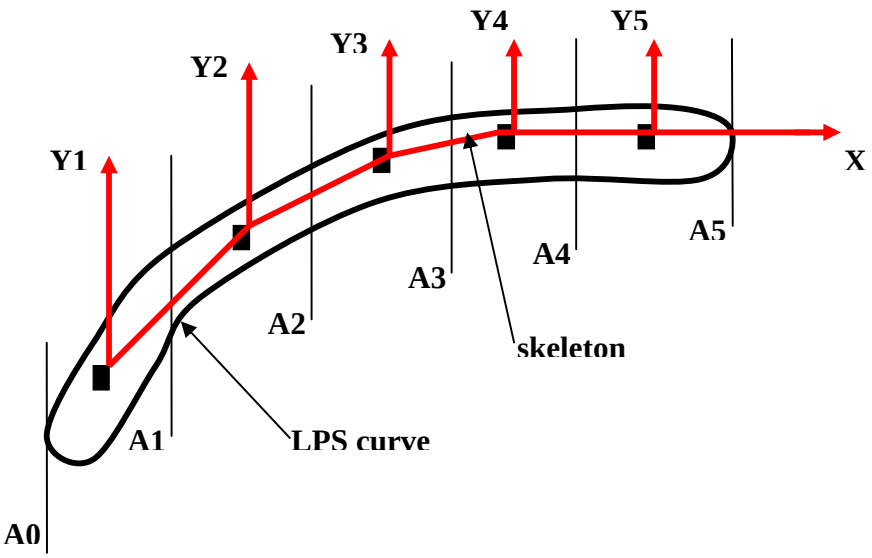

Figure 2.8: Generation of skeleton.

Let's denote Ym_i and Y_i - ordinates of i-th point of the skeleton of modulated and non-modulated LPS (i is also a number of slice in which this point is located), Nm_i and N_i - number of points in i-th slice, L - number of slices. The measure of similarity, based on skeletons of modulated and non-modulated LPS is defined as

$$\rho = \sqrt{\sum_{i=0}^{L-1} \left(Ym_i - Y_i\right)^2 \cdot \left(\left|Nm_i - N_i\right| + 1\right)}.$$

It is usual Euclid distance but with weights, which depend on the number of points in each slice. If the curves have different number of points in two corresponding slices, the difference between ordinates of skeleton in these slices is underlined by the difference between numbers of points.

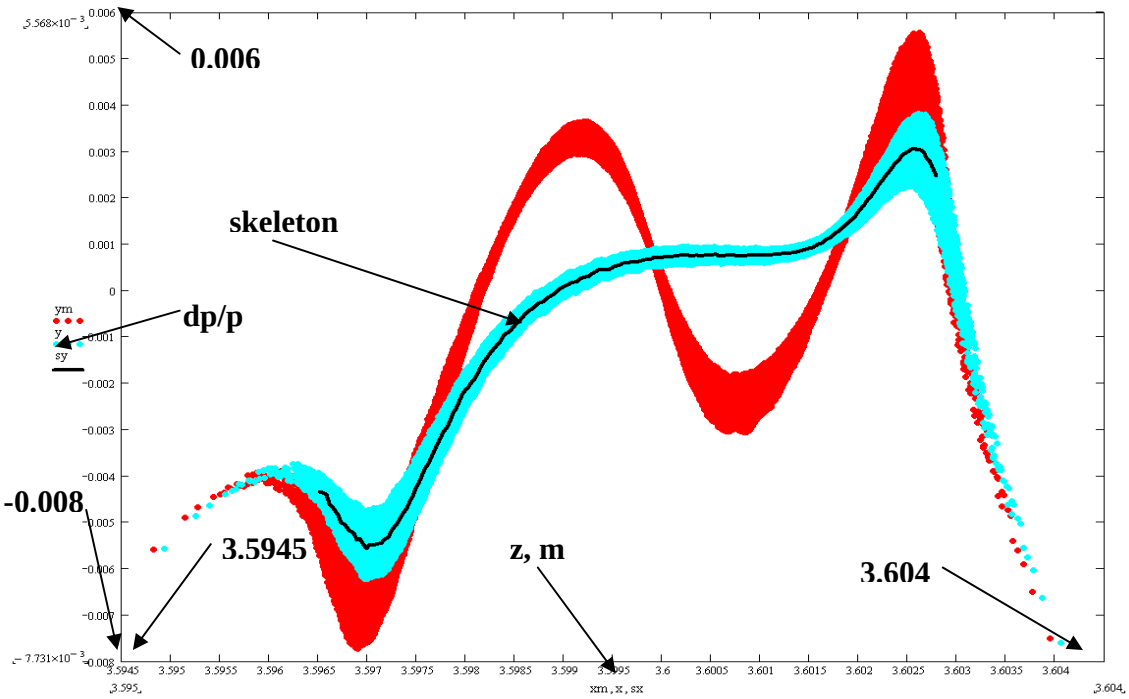

Figure 2.9: Modulated and non-modulated LPS with its skeleton, Q=0.10 nC.

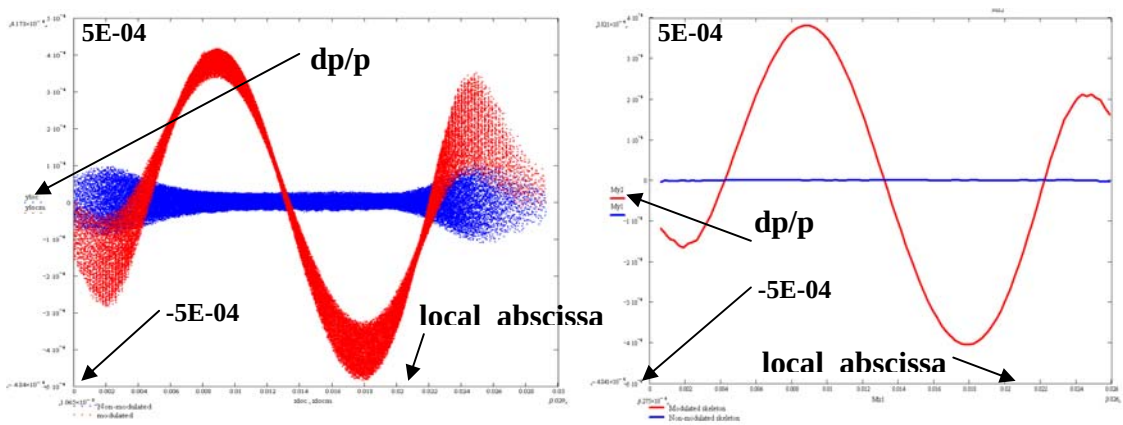

Figure 2.10: Straightened LPSs and their skeletons, Q=0.01 nC.

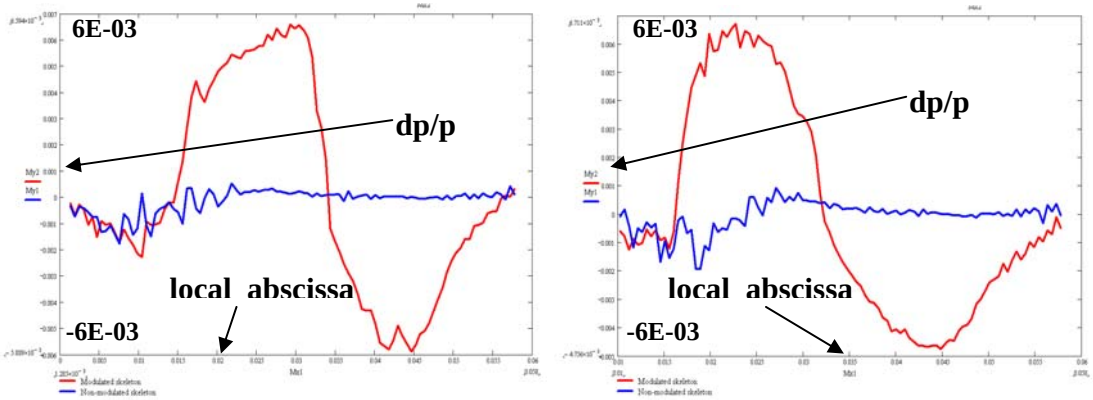

Figure 2.11: Examples of skeletons of straightened LPSs for Q=1.0 nC (left) and Q=1.5 nC (right).

However, it worth to note, that proposed procedure of straightening of LPS is rather rude because partition of highly nonlinear LPS is non-adaptive (that is, the grid is constant and doesn't conform to the peculiarities of the curve, figure 2.8). Nevertheless, this technique is sufficient for our purposes - to underline introduced modulations, distinguish the number of crests and evaluate measure of similarity based on ordinates of skeletons.

The plots of dependence of proposed weighted Euclid similarity measure on the charge for the case of: two crests with $depth = 0.5$ (red), two crests with $depth = 0.3$ (pink), three crests with $depth = 0.5$ (black) and three crests with $depth = 0.3$ (brown) are depicted in figure 2.12. The minimum value of the charge is 0.01 nC, maximum value is 1.55 nC, step-interval equals 0.04-0.05 nC.

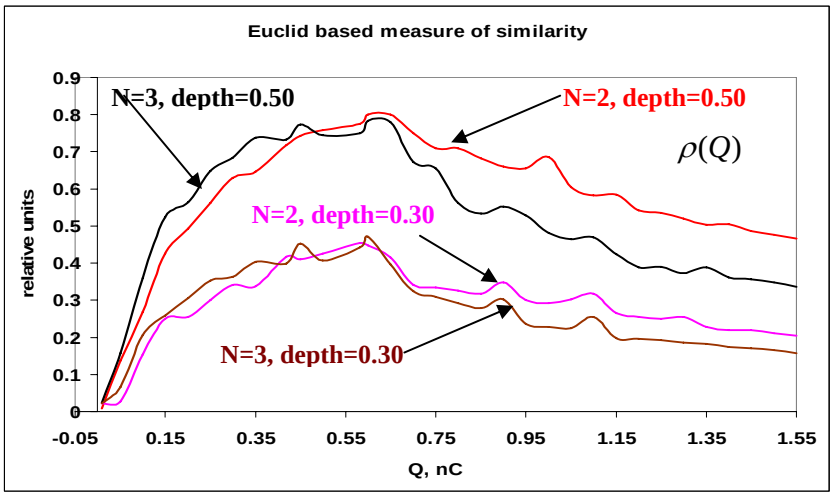

Figure 2.12: Dependence of weighted Euclid based similarity measure on the charge of the bunch.

As procedure of straightening is rude, some spikes occurred on graphs of Euclid based measure of similarity. In order to underline general trend, plots in figure 2.12 were smoothed using moving average of length 3 with equal weights. It can be seen from these plots, that our hypothesis about smearing effect with an increase of the charge is confirmed.

2.2.2 Emittance based measure of similarity

A statistical definition of the emittance is the so-called normalized rms emittance defined as [43]

$$\varepsilon_{n,rms} = \frac{1}{m_0 c}\sqrt{\left\langle z^2 \right\rangle \left\langle p_z^2 \right\rangle - \left\langle z p_z \right\rangle^2},$$

where $\langle\ \rangle$ defines the second central moment of the particle distribution

$$\left\langle z^2 \right\rangle = \frac{\sum z^2}{n} - \left(\frac{\sum z}{n}\right)^2, \quad \left\langle p_z^2 \right\rangle = \frac{\sum p_z^2}{n} - \left(\frac{\sum p_z}{n}\right)^2,$$

$$\left\langle z p_z \right\rangle = \frac{\sum z p_z}{n} - \frac{\sum z \sum p_z}{n^2},$$

and all sums are performed for the n particles in the distribution. $\varepsilon_{n,rms}$ is proportional to the area of the LPS ellipse.

It is obvious that if the LPS has additional modulations, emittance of such LPS will "catch" these modulations because its definition includes notions of the dispersion and covariation. Three measures, based on the values of the emittance, were used for investigation of the dependence of similarity between modulated and non-modulated LPS. One is given by the following formula and is very natural (it is emittance growth)

$$\rho_1^{\varepsilon} = \left|\varepsilon_{n,rms}^{m} - \varepsilon_{n,rms}^{nm}\right|,$$

where indexes m and nm stands for modulated and non-modulated cases correspondingly. The other measure can be calculated by formula

$$\rho_2^{\varepsilon} = \frac{\left|\varepsilon_{n,rms}^{m} - \varepsilon_{n,rms}^{nm}\right|}{\varepsilon_{n,rms}^{nm}}.$$

The last one is given by the formula

$$\rho_3^{\varepsilon} = -\ln\left(\frac{2\cdot\varepsilon_{n,rms}^{m}\cdot\varepsilon_{n,rms}^{nm}}{\left(\varepsilon_{n,rms}^{m}\right)^2 + \left(\varepsilon_{n,rms}^{nm}\right)^2}\right).$$

It is obvious, that

$$\frac{2\cdot a\cdot b}{a^2+b^2} \to \begin{cases} \in (0,1)\ \forall a,b>0 \\ =1 \Leftrightarrow a=b \end{cases}.$$

Usual measure of similarity equals zero if objects are the same and tends to infinity if objects completely different. That's why the second measure of similarity is written in such way (with negative logarithmic transform).

The plots of dependence of these measures on the charge for the case of: two crests with $depth = 0.5$ (red), two crests with $depth = 0.3$ (pink), three crests with $depth = 0.5$ (black) and three crests with $depth = 0.3$ (brown) are depicted in figure 2.13 (top - ρ_1^{ε}, middle - ρ_2^{ε}, bottom - ρ_3^{ε}). The minimum value of the charge is 0.01 nC, maximum value is 1.55 nC, step-interval equals 0.04-0.05 nC.

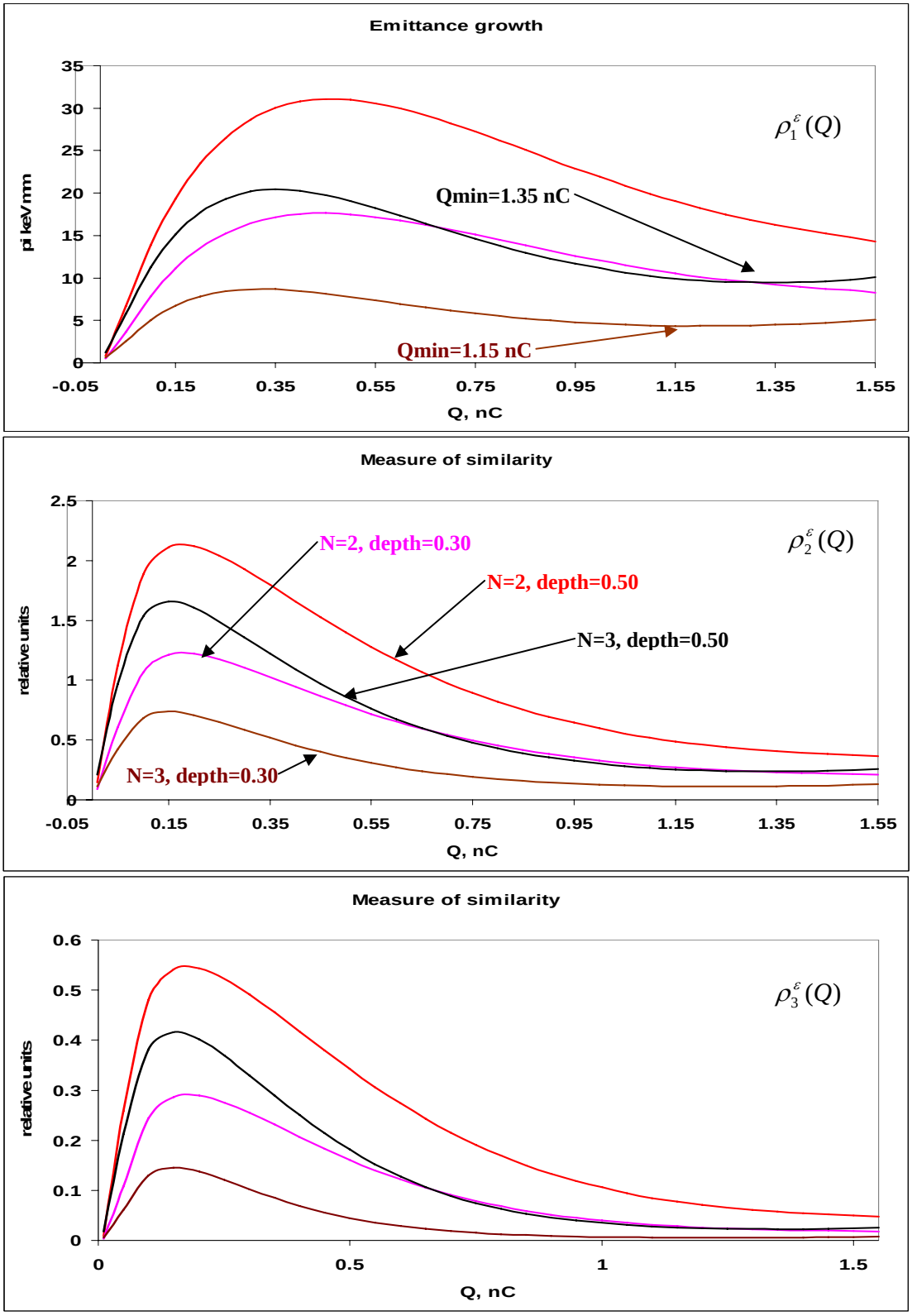

Figure 2.13: Dependence of emittance based measures of similarity on the charge of the bunch.

It can be seen from the figure 2.13 that the hypothesis is completely confirmed by these plots, especially with the plot of second and third measures of similarity – they turned out to be more sensitive to the mutual changes in the values of “modulated” and “non-modulated” emittance. Also, it can be observed, that with the decrease of the $depth$ or with the increase of the number of crests distance between modulated and non-modulated LPS decreases. An interesting feature can be distinguished, especially form the top plot of the figure 2.13 – curves for the case of three crests have prominent local minimum – 1.35 nC in case of $depth = 0.5$ and 1.15 nC in case of $depth = 0.3$. Most likely, curves for the case of two crests have also such maximum, but in the range of higher bunch charges. Thus, probably it is possible to find to some extent optimal value of charge, which, on the one hand, will be enough for experiments and on the other hand will provide the highest smearing effect.

So, because plots with different measures of similarity show the same behaviour for different values of modulation amplitude and frequency, we can come to a conclusion, that our hypothesis, that initial modulations of the temporal intensity distribution of laser pulse can be smeared out with the increase of the electron beam charge, is correct. Moreover, plots of emittance based similarity measure for the case of three crests clearly show local minimum.

2.3 Simulations with booster cavity

Though the suppression a space charge induced emittance growth by fast beam acceleration with high RF gun gradients can be done, the space charge blows up the emittance after the RF gun. To prevent this emittance growth a booster cavity has to be used for fast acceleration. Therefore, it is necessary to investigate how modulations of initial longitudinal distribution of the electron bunch will impact onto the profile of the LPS after booster cavity. Also, as booster cavity is installed at PITZ, it is interesting to compare simulated and experimental results (PITZ Logbook, August 18th, 2005, night shift). In figure 2.14 there is a plot of a real laser profile with flat-top fit (top; two crests clearly can be seen; modulation amplitude is about 40%) and two plot of momentum distributions for Q=0.55 nC (middle) and for Q=1.20 nC (bottom); Gun SPPhase=-103 deg and Booster SPPhase=+2deg (SPP – set point phase – is related to a real mathematical phase via some shift). Two peaks of momentum distribution smear out with the increase of the electron beam charge. This means, that in principle, initial intensity modulations of the laser pulse also smear out. Additionally, in figure 2.15 there is an example of real laser profile with three crests (top) and momentum distribution (bottom). It clearly can be seen, that modulated laser profile leads to modulated momentum distribution with also three crests. Using ASTRA, the plots of LPS and momentum distribution, which show in qualitative manner the same behavior, as in figure 2.14, were obtained for Q=0.1 nC and Q=0.7. They are depicted in figure 2.16. Momentum distribution of the electron bunch after booster cavity has two peaks and smears out with the increase of the bunvh charge (initial intensity laser distribution had two crests and its amplitude was $depth = 0.5$).

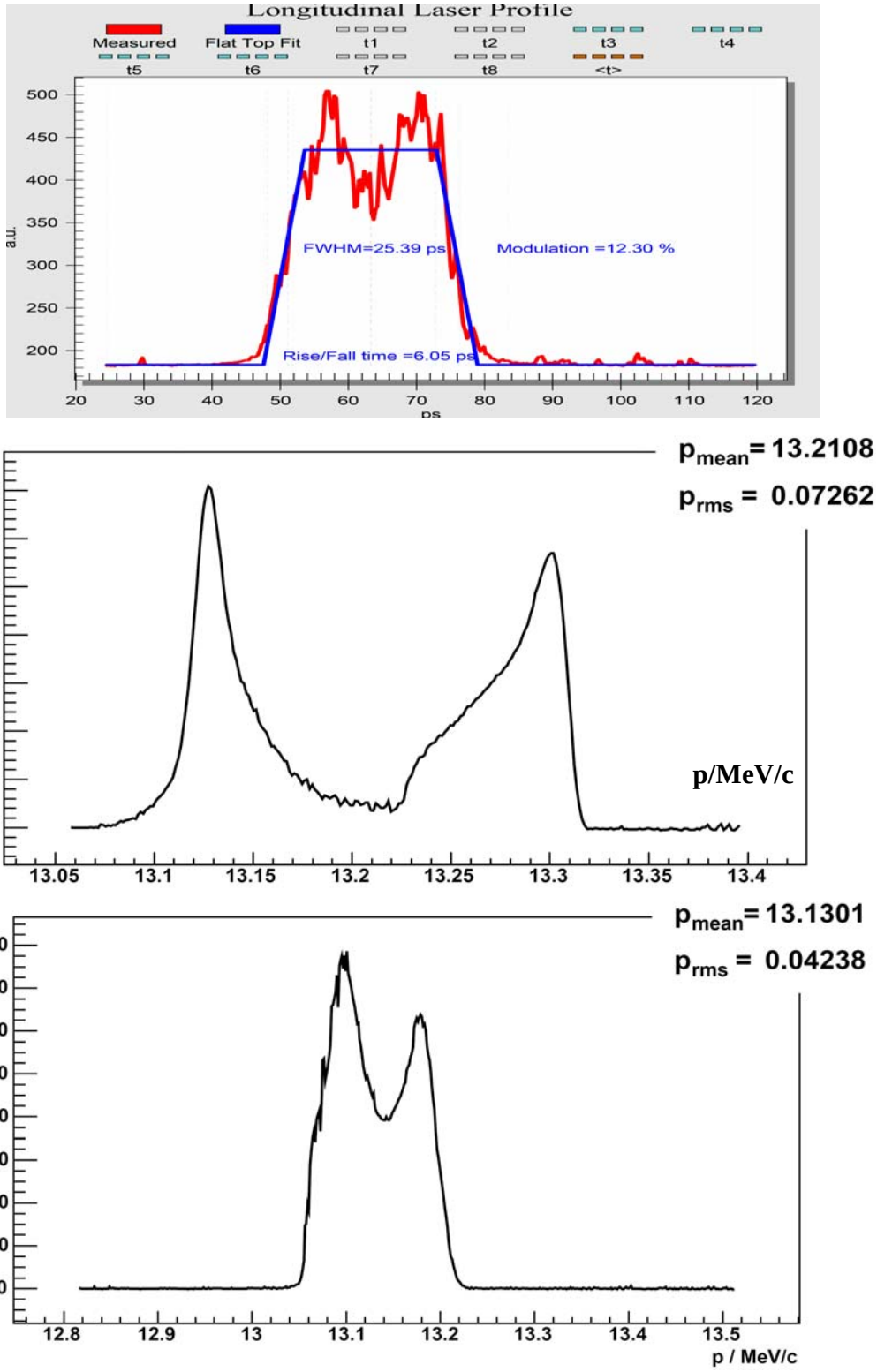

Figure 2.14: Example of experimentally observed laser intensity distribution (top) and momentum distribution for Q=0.55 nC (middle), Q=1.20 nC (bottom). Note, that range of the horizontal axis at two low plots is different.

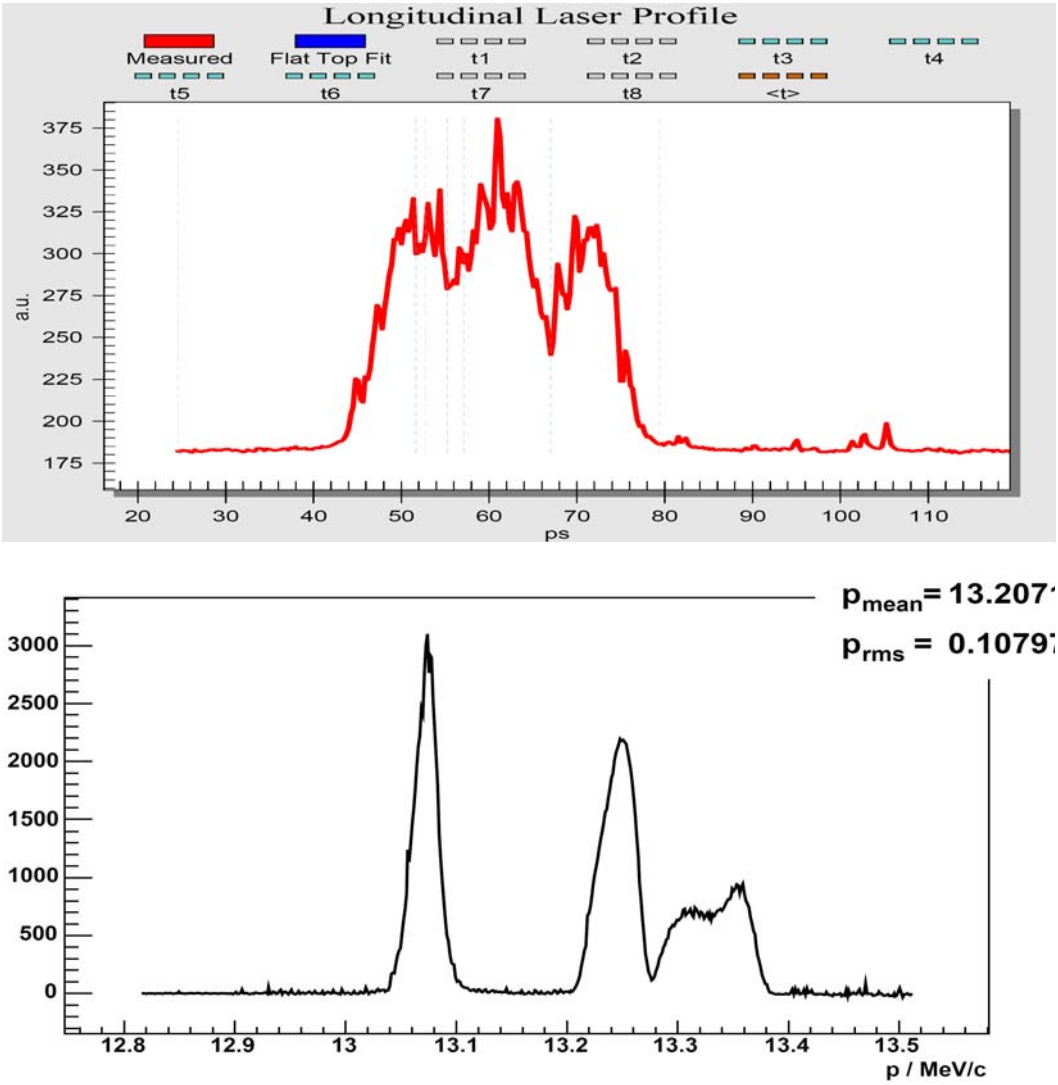

Figure 2.15: Example of experimentally observed laser intensity distribution (top) and momentum distribution (bottom) for Q=0.55 nC.

These two simulation results show that local energy modulations after booster cavity have been introduced. Thus, initial modulated density distribution of the laser beam leads to energy modulations after accelerator and, as [38] predicts, this can lead to significant distortions of LPS and emittance growth. These simulation results also confirm our hypothesis about smearing affect.

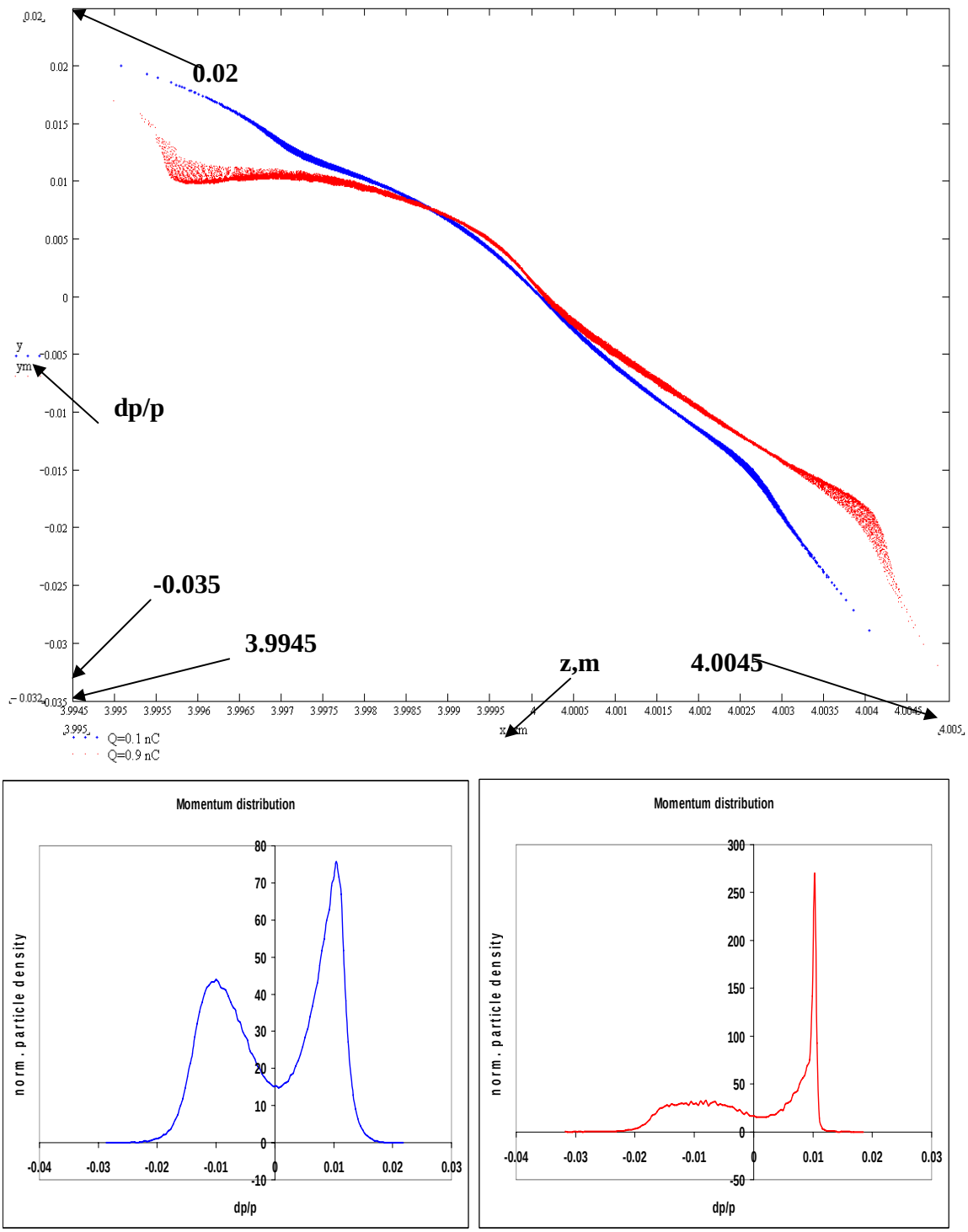

Figure 2.16: Simulated modulated LPSs after booster (top) and momentum distributions for Q=0.1 nC (left) and Q=0.7 nC (right).

3 Conclusions

3.1 Possible explanations of observed phenomenon

Two effects might be possible for smearing of introduced modulations. One of them is that if the space charge of the emitted bunch is high, it induces also high positive mirror charge on the cathode, which can smooth out local density variations directly after cathode. To check this explanation longitudinal distribution just after cathode (ZSTOP~5 cm) and at the end of the gun cavity (ZSTOP~25 cm) for Q=0.01, 0.5, 1.0, 1.5 nC was calculated (figure 3.1). It can be observed from this picture, that directly after the cathode induced positive charge in fact smears out longitudinal distribution with the increase of the electron beam charge. In other words mentioned explanation is confirmed by simulations. Also, it is worth to mention, that after additional 20 cm of travel in RF gun cavity the shape of longitudinal distribution doesn't change much for corresponding values of the electron charge. This clearly confirms, that high RF gun gradients prevent from space charge induced emittance growth of the electron beam. However, because after RF cavity simulations showed, that LPS continue to smear out, this observation indicates, that additional smearing effect could take place.

A simple "two-gaussian-particles" model might explain the additional smearing effect, which takes place during the travel of electron beam after the RF gun cavity, is the following. Let's go to the reference frame connected with moving electron bunch and consider modulated charge distribution as if it equals sum of two equal gaussian densities which centers are symmetrically located w.r.t. zero. Let L - the distance between centers and σ - rms length of distributions. Example of such distributions is depicted in figure 3.2. It is obvious, that the model can be parameterized in such way, that all quantities will depend only on the ratio L/σ. Let's consider some point **D** of the density **I**. On the one hand, density **I** and density **II** will repel each other as ordinary negative particles and the points **A** and **B** will disperse. As a consequence of such movement, the point **C** will go down. This repulsion is responsible for the net force **F2,** acting on the point **D.** On the other hand (especially with high values of the charge) particles in each density **I** or **II** will repel each other and this will cause rms length growth of both densities - these interactions are responsible for the net force **F1** acts on the point **D**. As a consequence of these interactions, the point **C** will go up. Also, e.g., density **II** can affect the right side of density **I** stronger, than left side. In such case the density **I** will contract. These are the main changes that can occur due to Coulomb forces. If the resulting movement of the point **C** will be up – this will lead to the smearing effect. The same, but in terms of forces, means, that **F1** should be greater than **F2** for points in left half of the density **I** and vice versa for smearing effect to occur. It is worth to note, that resulting forces are fully determined by space charge density. Thus, influence of all mentioned effects should be estimated depending on the ratio L/σ and the value of electron bunch charge. This model, being simple, however can explain additional smearing effect, which was observed during simulations.

Let's use this "two-gaussian-particles" model to explain the smearing effect due to positive induced mirror charge on the cathode. In figure 3.3 the illustration is depicted. Charge density of the positive mirror charge is symmetrical with reference to the zero point of coordinate system. Let's consider some point **D** of the density of the negative charge, emitting from the cathode. Force **F1** acts on this point because of positive mirror charge of

the cathode. Also, force **F2** acts on this point due to repulsion of particles of the density. It is obvious, that these forces provoke the smearing effect, which much more pronounced than in previous case, as these forces have the same direction.

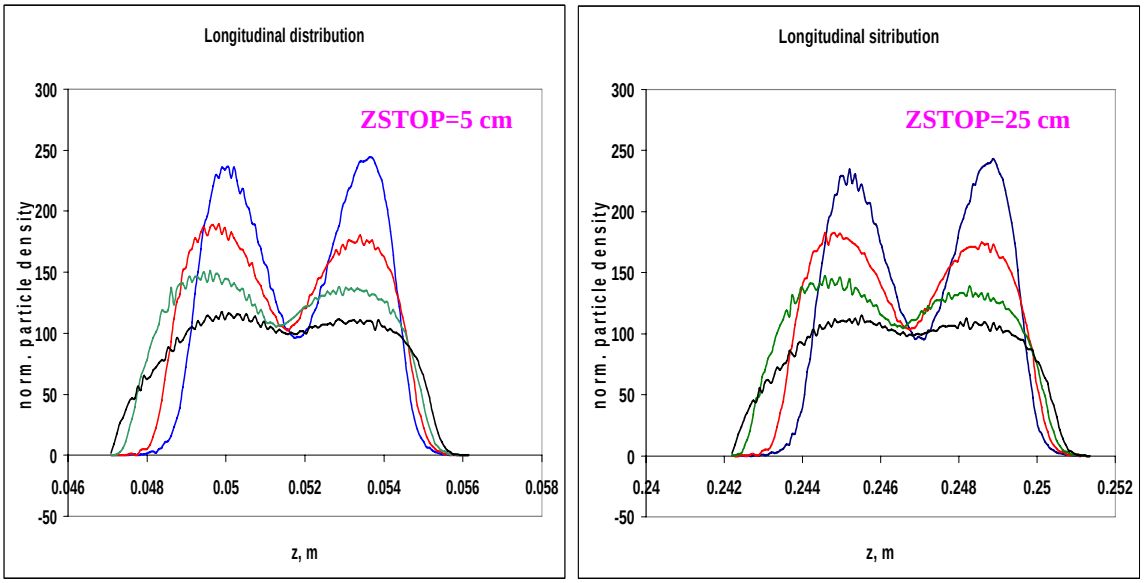

Figure 3.1: Examples of the longitudinal distribution for Q=0.01 nC, Q= 0.5 nC, Q=1.0 nC, Q=1.5 nC and ZSTOP=5 cm (left), ZSTOP=25 cm (right).

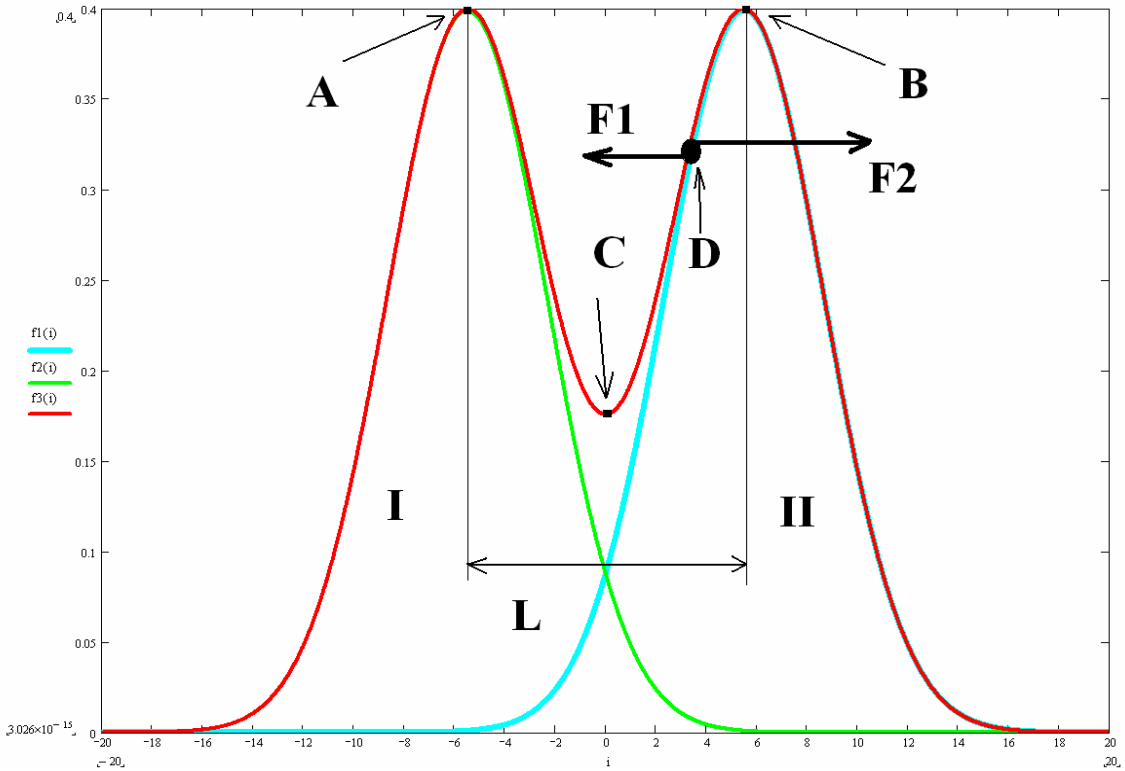

Figure 3.2: Illustration of "two-gaussian-particles" model for the case of additional smearing effect.

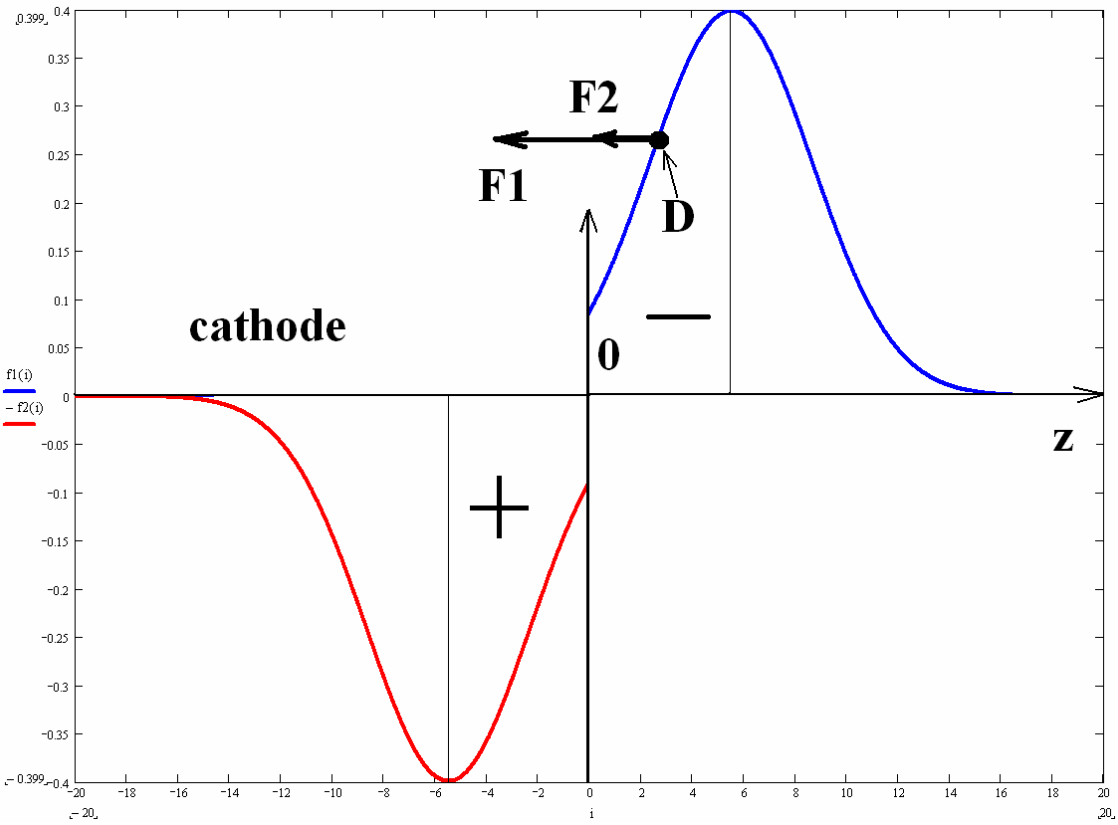

Figure 3.3: Illustration of "two-gaussian-particles" model for the case of positive mirror cathode charge effect.

3.2 The main results

- Method for generation of modulated temporal density distribution of laser pulse has been developed
- Concepts of skeletons, skeleton-based straightened version of LPS, which can underline introduced modulations, were elaborated.
- Simulations of modulated LPS for different values of electron bunch charge, modulation amplitude and frequency have been performed.
- Different measures of similarity, based on notions of skeleton and emittance, were introduced and their behavior, depending on electron bunch charge, modulation frequency and amplitude was investigated and discussed, namely these measures decrease with the increase of the electron bunch charge. This confirms initial hypothesis.
- "Noisy" spikes of ASTRA's generator were detected and their spectral content was investigated.
- Simulations with booster cavity were done and results were compared with real experimental observations.
- Explanation of observed phenomenon was proposed.

3.3 Directions for future research

- It is necessary to investigate the impact of modulations for larger range of parameters such as modulation frequency and amplitude, electron bunch charge. Also, simulations should be done for different set-ups (e.g., with additional booster, with dispersive arm); parameters of simulations should be tuned in such a way to resemble a real experiment set-up of PITZ.
- Adaptive technique for straightening of LPS could be worked out.
- Maybe, other concepts of distance should be elaborated, which can underline certain features of similarity\dissimilarity between modulated and non-modulated LPSs.
- Theoretical models (probably, based on ideas, mentioned in the above section), which can explain the smearing effect, should be built and their estimates should be compared with the experimental and simulation results.

Acknowledgements

First of all I'd like to thank my supervisor, Mikhail Krasilnikov for help and very useful discussions. Without his right ideas and remarks my report wouldn't be done.

I want to thank Juliane Roensch for being very kind – she gave me her routines. Without them I wouldn't be able to draw such nice plots.

Also, I want to thank all members of PITZ group for creative atmosphere and summer student for being good colleagues.

Last but definitely not the least many thanks go to Dr. Hiller and Mrs. Baer for organizing the summer student program. Everything was well planned. I had a great experience during the program.

Appendix A

generator.in:

```
&INPUT
FNAME='rfgun.ini'
IPart= 50000
Species='electrons'
Probe=.True.
Noise_reduc=.T.
Cathode=.T.
HIGH_RES=.T.
Q_total=0.01E0
Ref_zpos=0.0E0
Ref_clock=0.0E0
Ref_Ekin=0.0E0
Dist_t='p'
Dist_z='p'
Lt=22.4E-3
rt=4.3E-3
Dist_pz= 'i',
LE= 0.00055
emit_z=0.00E0
cor_Ekin=0.E0
Dist_x='radial'
sig_x=0.575E0
Dist_px='g'
Sig_px=0.0
cor_px=0.0E0
Dist_y='r'
sig_y=0.575E0
Dist_py='g'
Sig_py=0.0E
Nemit_y=0.0E0
cor_py=0.0E0
LPROMPT=.F
/
```

rfgun.in:

```
&NEWRUN
Head='rfgun'
RUN= 1
Loop=F,
Nloop=2
Distribution='rfgun.ini',
Xoff=0.0,
Yoff=0.0
Lmagnetized=.F
EmitS=.T
PhaseS=.T
TrackS=.F
RefS=.F
TcheckS=.T
CathodeS=.T
TRACK_ALL=.T,
PHASE_SCAN=.F,
LANDFS  = .T,
AUTO_PHASE=.T
check_ref_part=.F,
ZSTART=0.0,
ZSTOP=3.60
Zemit=1000
Zphase=10
H_max=0.001
H_min=0.0001
Lmonitor=.F
LPrompt=.F
Qbunch=0.01E0
\
&CHARGE
LSPCH=T
Nrad=20,
Nlong_in=150
Cell_var=2.0
min_grid=0.4D-6
Max_scale=0.05
Max_count=100
\
Lmirror=.T
&Aperture
LApert= .F
File_Aperture='app.txt'
&CAVITY
LEFieLD=.T
FILE_EFieLD(1)='efld.dat',
Nue(1)=1.3,
MaxE(1)=-42.0,
Phi(1)= -1.74
C_pos(1)=0.0,
&SOLENOID
LBFieLD=.T,
FILE_BFieLD(1)='MainSol.txt',
S_noscale(1)=.F.
MaxB(1)= 0.1748
S_pos(1)=0.0,
S_xoff(1)=0.0,
S_yoff(1)=0.0
FILE_BFieLD(2)='BuckSol.txt',
S_noscale(2)=.F.
MaxB(2)= -8.67647E-003
&QUADRUPOLE
Lquad=.F
```

Additional parameters for booster cavity in namelist CAVITY:

```
File_Efield(2) = 'TeSLA_1_9cells.efld',
Nue(2)=1.300,
MaxE(2)= 26.2687
Phi(2)= -15.631
C_pos(2)=2.99427
```

In case of booster cavity ZSTOP=4.0.

Appendix B

The number of crests is equal to N=3. Plots for lower modulation amplitude were not depicted as they shows the same behaviour, the only difference is that modulations smear out faster.

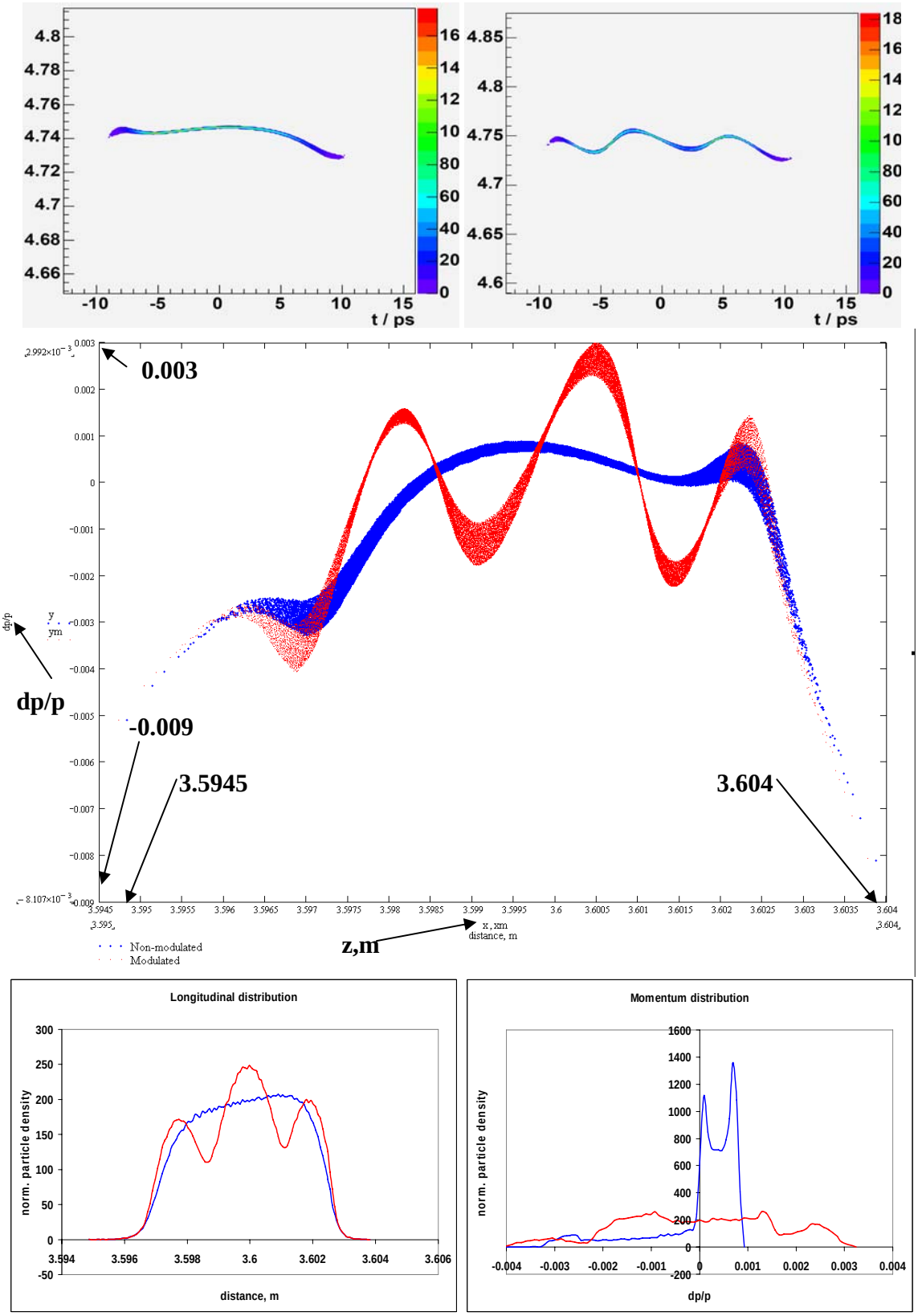

Figure B.1: Q=0.05 nC.

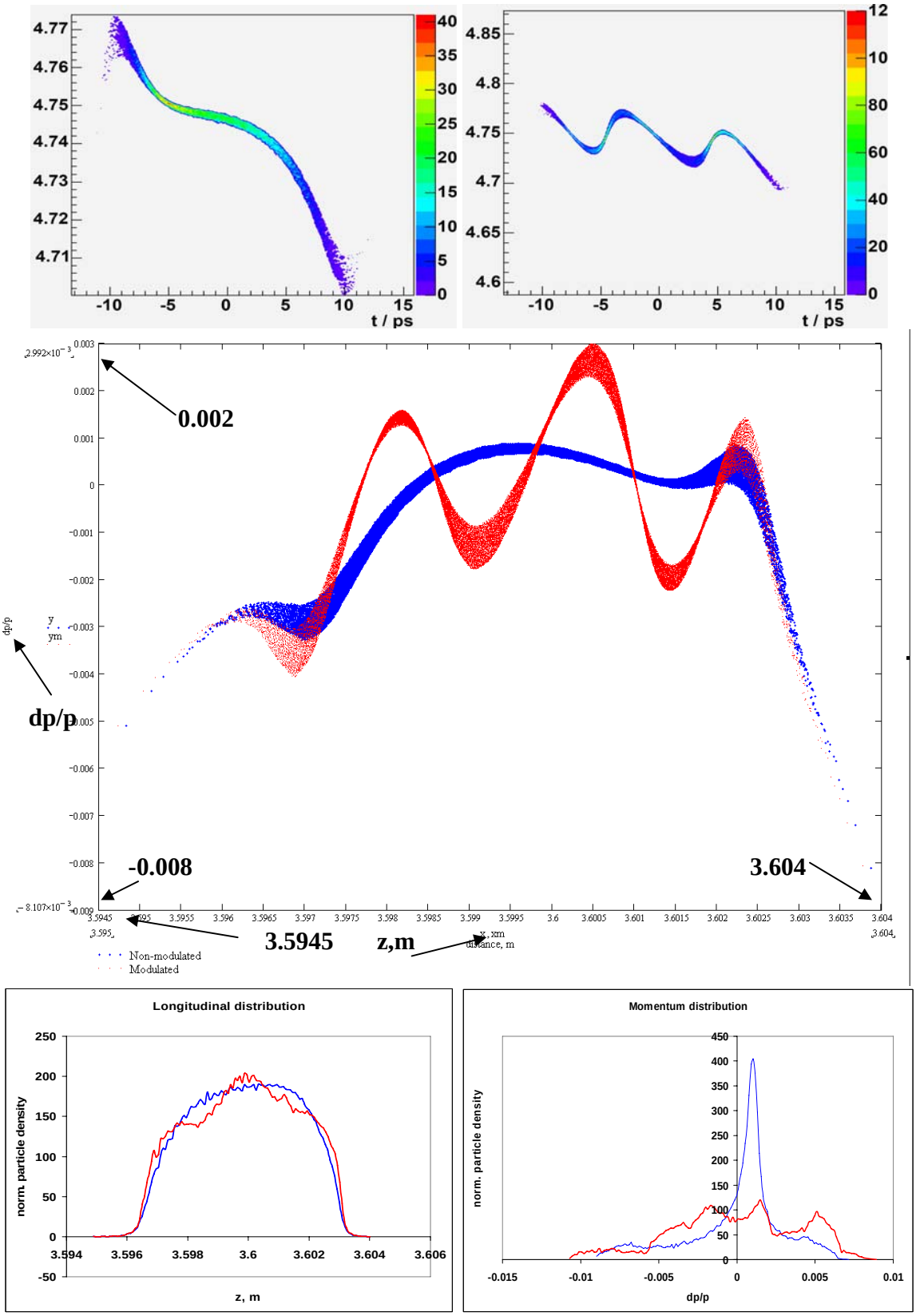

Figure B.2: Q=0.15 nC.

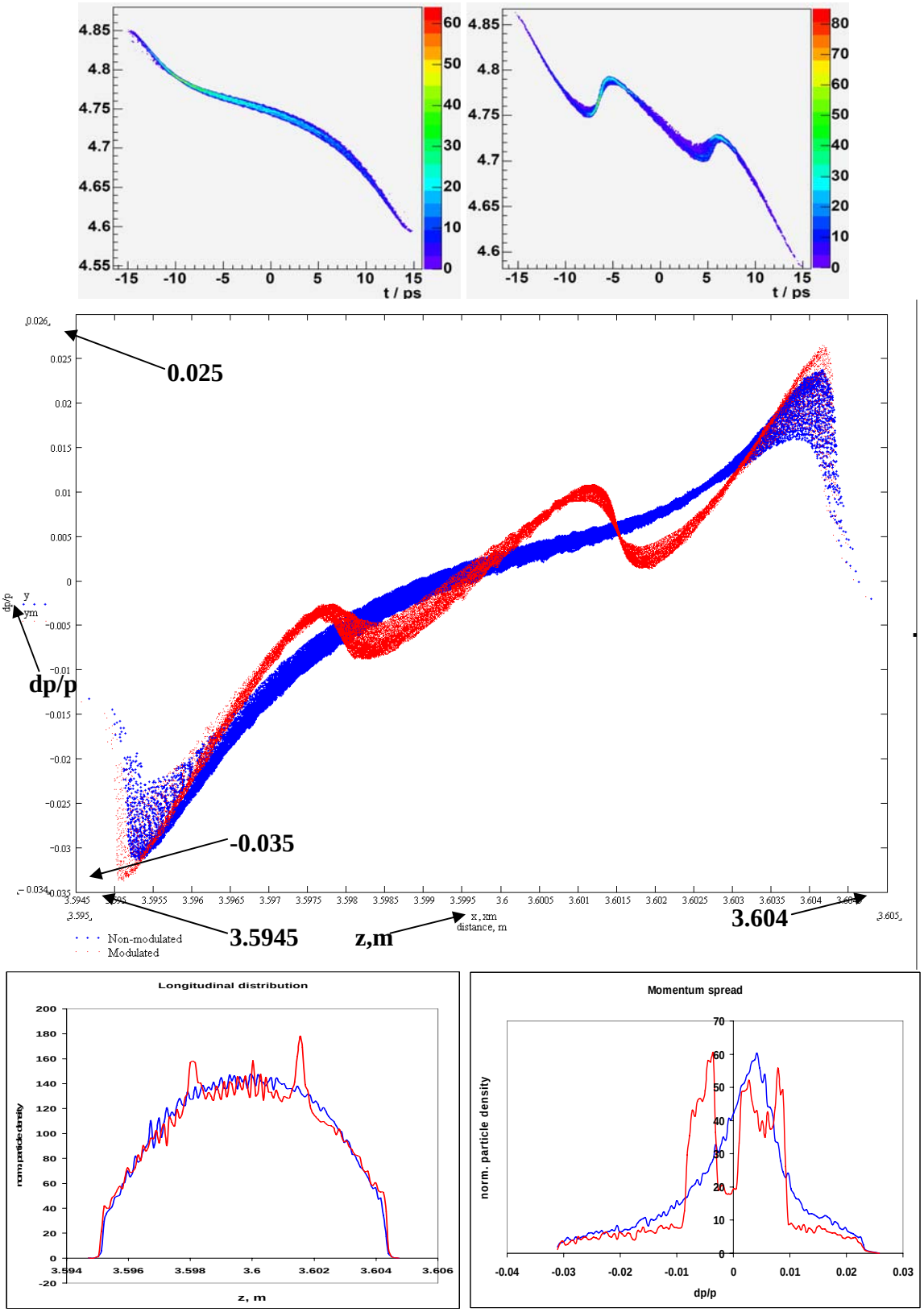

Figure B.3: **Q=0.70 nC.**

Appendix C

In this section “noisy” spikes of ASTRA’s generator are investigated. In figure C1 there is example of modulated LPS with “noisy” spikes. To produce modulated density distribution of laser beam the following technique initially was used. First of all, modulated flat-top histogram with the same parameters (FWHM, raise time), as in non-modulated case, was produced (like in section 2.1). Then, using quasi-random generator from MathCAD, a point (x, y) with i.i.d. coordinates, uniformly distributed onto the square (which included this modulated flat-top histogram), was generated. If this point was also included into the interior of modulated flat-top histogram, its abscissa was taken as a start time for particle from cathode. A column of 50000 such values was generated and included in the output file of generator.exe instead of **clock** column.

It was supposed that because generator.exe generates particle coordinates quasi-randomly following a Hammersley sequence [45], proposed procedure for generation of modulated intensity distribution of laser beam can break this quasi-randomness. That’s why “noisy” spikes appeared. Such spikes can distort introduced modulations and, consequently, prevent from right conclusions during research. Thus other technique for generation of modulated density distribution was elaborated.

In order to check this supposition and investigate “noisy” spikes Noise_reduc parameter in the file generator.in must be FALSE. It is the same as to “break” quasi-randomness in a way as it was discussed above. In figure C2 there is an example of usual straightened LPS, straightened LPS with spikes (Noise_reduc=FALSE) and skeletons of these two straightened LPS for Q=0.01 nC.

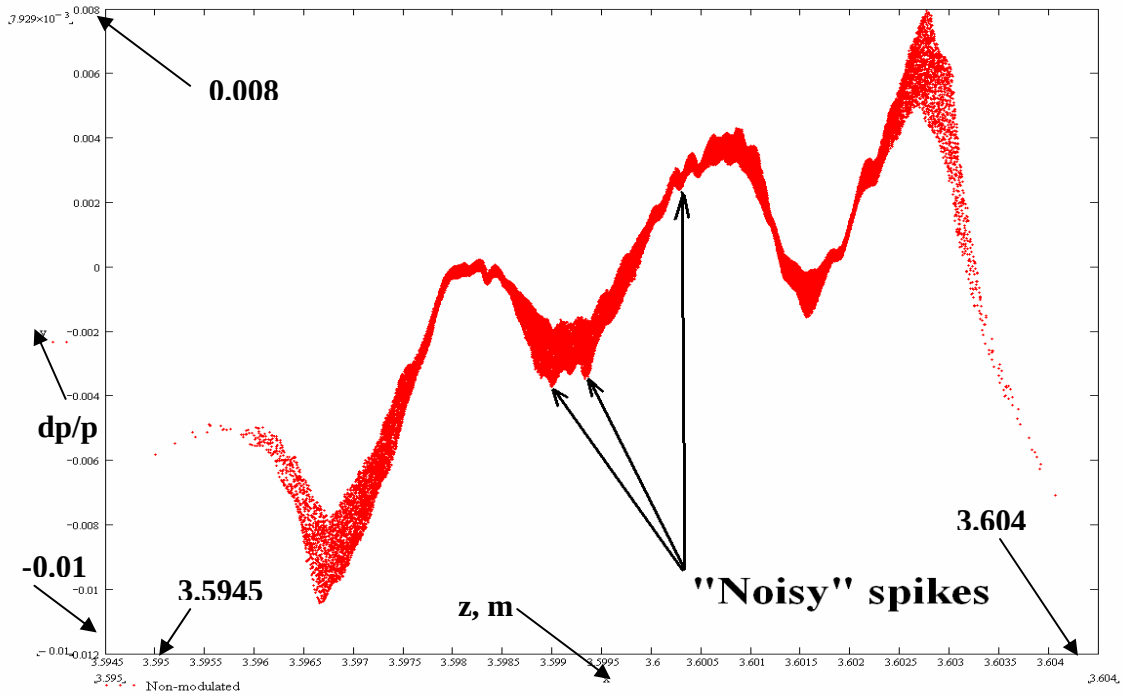

Figure C1: Example of modulated LPS (three crests, $depth = 0.5$, Q=0.15 nC) with “noisy” spikes.

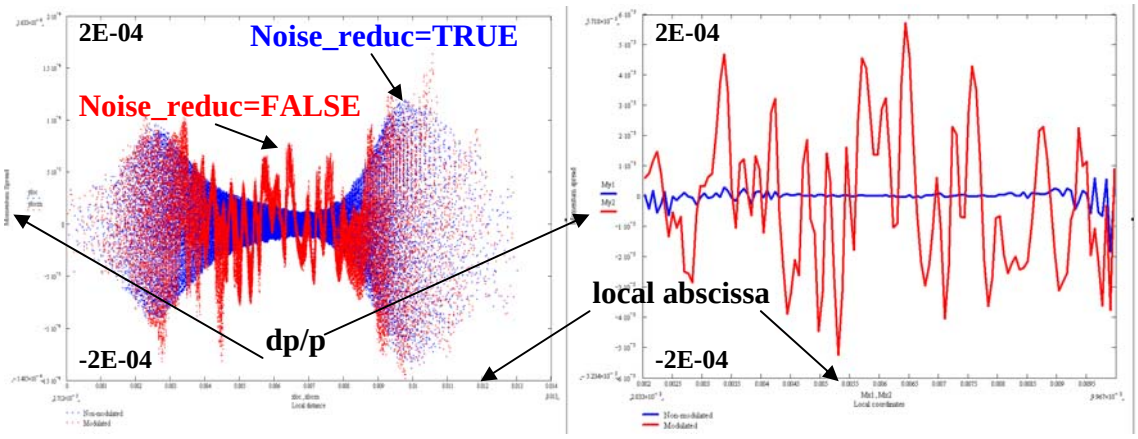

Figure C2: Examples of "noisy" straightened LPSs and their skeletons for Q=0.01 nC.

From the skeleton of "noisy" LPS it can be observed, that these spikes resemble autoregression process (presumably, the second order autoregression process) with white noise. Usual Fourier spectrum [46] was used to resolve spectral content of the signal (figure C3) and confirm this observation [46].

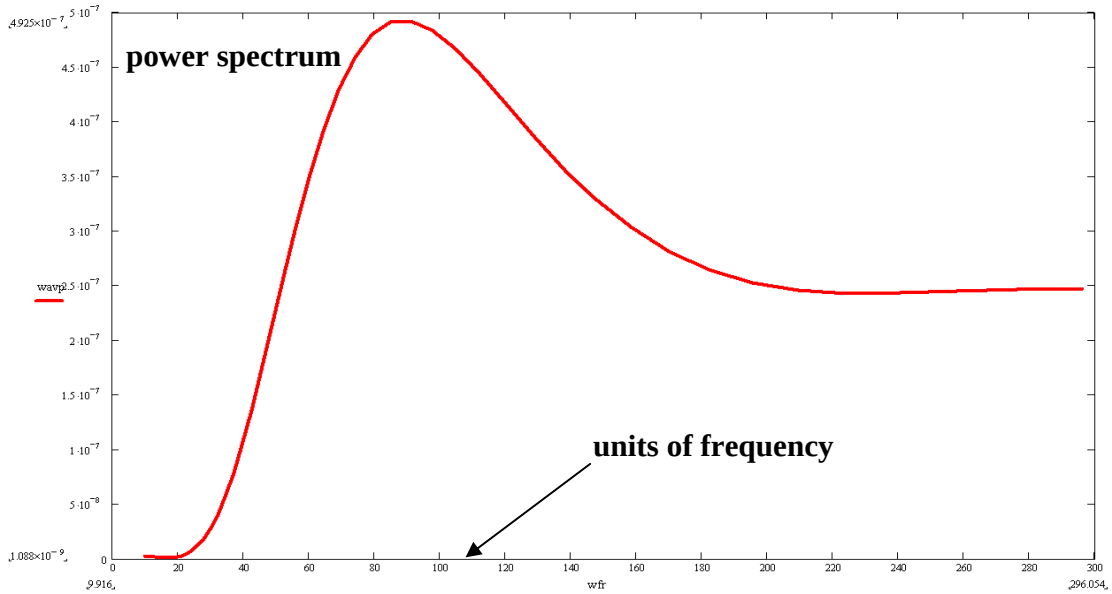

Figure C3: Fourier spectrum of "noisy" skeleton for Q=0.01 nC.

In order to investigate frequency content more thoroughly, such transform should be used, that has both resolutions in time and frequency. A wavelet continuous spectrum analysis meets these requirements [44]. Continuous wavelet transform is defined as [45]

$$W(s,t) = \int_{-\infty}^{+\infty} f(\tau)\psi_{s,t}(\tau)\,d\tau,$$

where $\psi_{s,t}(\tau) = \frac{1}{\sqrt{s}}\psi\left(\frac{\tau - t}{s}\right)$ - shifts and scaling of square integrable wavelet function $\psi(t)$, s - scale (approximately, it is inversely proportional to usual Fourier frequency), τ - shift parameter and $f(t)$ - considered signal. Admissibility conditions of wavelet function are listed in [44]. Usually, they are very general. To gain precise information about high-frequency components of the signal information should be extracted from short time intervals and vice versa. Usual Fourier transform doesn't allow such adaptability, because the bases functions, that are used, have infinite support. As the Fourier transform of $\psi_{s,t}(\tau)$ is equal to $\hat{\psi}_{s,t}(\omega) = s^{-3/2} \cdot e^{-i\cdot\tau\cdot\omega} \cdot \hat{\psi}(s\omega)$, it is clear, that if the wavelet function have compact support or decays fast, such adaptability will be obtained. In this report DOG wavelet with two vanishing integrals was used:

$$\psi(x) = \left(\frac{4}{3\sqrt{\pi}}\right)^{1/2} \cdot e^{-\frac{x^2}{2}} \cdot (1 - x^2).$$

In such case connection between Fourier frequency and scale is given by the formula

$$f_s = \frac{\sqrt{\pi}}{2^{3/2} \cdot \pi \cdot s}.$$

Absolute values of wavelet coefficients $W(s,t)$ were used as wavelet spectrum. In figure C4 there is wavelet (DOG wavelet was used, number of vanishing integrals equals to two) spectrum of "noisy" skeleton. Wavelet spectrum clearly shows the spectral content of the skeleton. It really resembles wavelet spectrum of autoregression process [47].

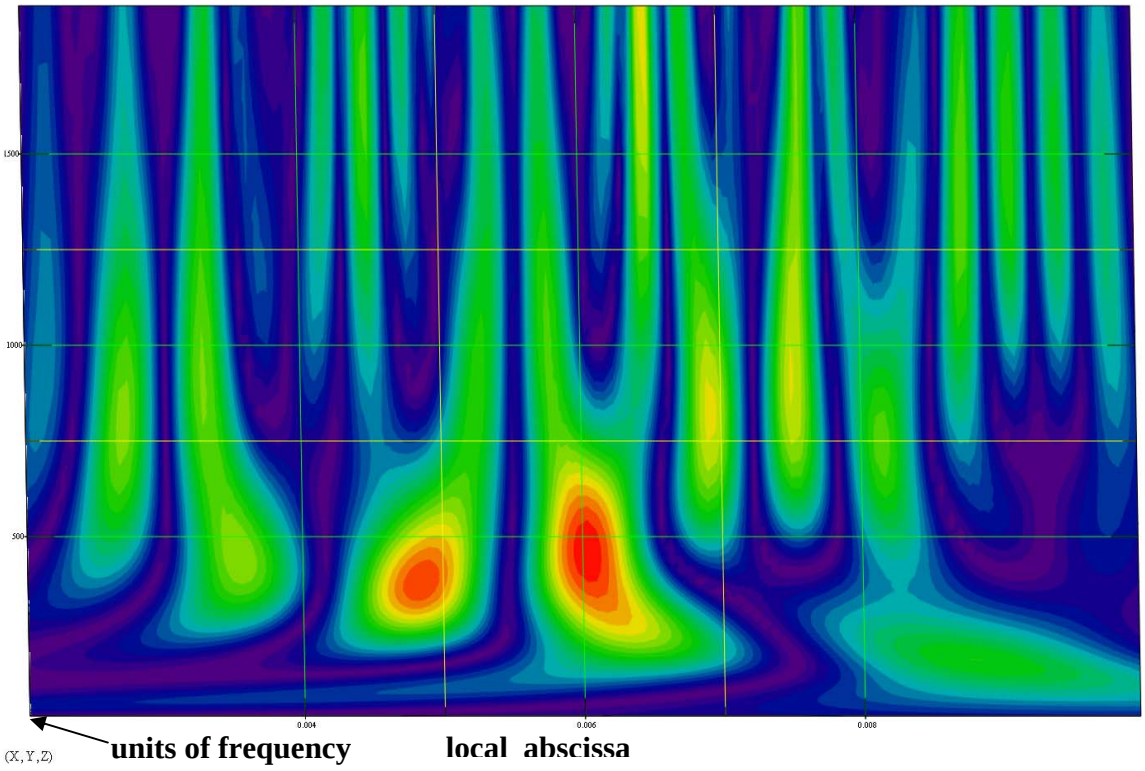

Figure C4: Wavelet spectrum of "noisy" skeleton for Q=0.01 nC.

References

[1] Linac Coherent Light Source (LCLS) Conceptual Design Report, SLAC-R-593, SLAC (2002).

[2] TESLA XFEL: First Stage of the X-ray Laser Laboratory (Technical Design Report, Supplement), TESLA FEL 2002-09, DESY (2002).

[3] Fawley W. et al., in Proceedings of the 2003 Particle Accelerator Conference, Portland, OR (IEEE, Piscataway, NJ, 2003), p. 923.

[4] Grave W. et al., in Proceedings of the 2003 Particle Accelerator Conference, Portland, OR (IEEE, Piscataway, NJ, 2003), p. 959.

[5] Schreiber S. et al., Properties of Cathodes Used in the Photoinjector RF Gun at the DESY VUV-FEL, EPAC 2003.

[6] Floettmann K., Stephan F., RF Photoinjectors as Sources for Electron Bunches of Extremely Short Length and Small Emittance, Proposal for the BMBF, 1999.

[7] http://desyntwww.desy.de/pitz/scientific_infos.html

[8] Roensch J., Selected Studies of the Longitudinal Phase Space at the Photo Injector Test Facility at DESY Zeuthen, diploma thesis, 2005.

[9] Stephan F. et al., Recent Results and Perspectives of the Low Emittance Photo Injector at PITZ, FEL 2004.

[10] Krasilnikov M. et al., Recent Developments at PITZ, PAC 2005.

[11] private communications with Mikhail Krasilnikov.

[12] Schreiber S., Laser for Injector III, TTF2 Review Meeting, Salzau, Germany, January 2003.

[13] Graves W. et al., Ultrashort Electron Bunch Length Measurements at DUVFEL, in Proceedings of the 2001 Particle Accelerator Conference, Chicago, IL, p. 2224.

[14] Huning M. et al., Observation of Longitudinal Phase Space Fragmentation at the TESLA Test Facility Free-Electron Laser, Nucl. Instrum. Methods Phys. Res., Sect. A 475, 384 (2001).

[15] Wang D.Z. et al., Phys. Rev. E 57, 2283 (1998).

[16] Loos H. et al., Experiments in Coherent Radiation at SDL, in Proceedings of the 2002 European Particle Accelerator Conference, Paris, 2002, p. 814.

[17] Shaftan T., Huang Z., Experimental Characterization of a Space Charge Induced Modulation in High-brightness Electron Beam, Phys. Rev. ST Accel. Beams 7, 080702 (2004).

[18] Braun H.H. et al, Emittance Growth and Energy Loss due to Coherent Synchrotron Radiation in a Bunch Compressor, Phys. Rev. ST Accel. Beams 3, 124402 (2000).

[19] Piot Ph. et al., Proceedings of EPAC 2000, Vienna, Austria, 2000, pp. 1546-1548.

[20] Li R., Proceedings of the EPAC 2000, Vienna, Austria, 2000, pp. 1312-1314.

[21] Rossbach J., A VUV Free Electron Laser at the TESLA Test Facility at DESY, Nucl. Instrum. Methods Phys. Res., Sect. A 375, (1996) 269-273.

[22] Saldin E.L. et al., An Analytical Description of Longitudinal Phase Space Distortions in Magnetic Bunch Compressors, Nucl. Instrum. Methods Phys. Res., Sect. A 483, (2002) 516-520.

[23] Saldin E.L. et al., Longitudinal Phase Space Distortions in Magnetic Bunch Compressors, DESY report 01-129, 2001.

[24] Saldin E.L. et al., Klystron Instability of a Relativistic Electron Beam in a Bunch Compressor, Nuclear Instruments and Methods Phys. Res., Sect. A 490, 1 (2002).
[25] Limberg T. et al., An analysis of Longitudinal Phase Space Fragmentation at the TESLA Test Facility, Nucl. Instr. and Meth. Phys. Res., Sect. A 475, (2001) 353-356.
[26] Huang Z. et al., SLAC-PUB-9818, 2003.
[27] Huang Z. et al., SLAC-PUB-9538, 2002.
[28] Derbenev Ya.S., TESLA-FEL 95-05, 1995.
[29] Limberg T., Numerical Investigations of CSR Driven Instability in Magnetic Bunch Compressors, EPAC 2002.
[30] Heifets S. et al., SLAC-PUB-8988, 2001.
[31] Stupakov G. et al., SLAC-PUB-8761, 2001.
[32] Derbenev Ya.S. et al., SLAC-PUB-7181.
[33] Huang Z. et al., Phys. Rev. ST Accel. Beams 5, 074401 (2002).
[34] Heifets S. et al., Phys. Rev. ST Accel. Beams 5, 064401 (2002).
[35] Huang Z. et al., Nucl. Instr. and Meth. Phys. Res., Sect. A 528, (2004) 345-349.
[36] Reiche S. et al., Phys. Rev. ST Accel. Beams 6, 040702 (2003).
[37] Limborg-Deprey C. et al., Computation of the Longitudinal Space Charge Effect in Photoinjectors, EPAC 2004.
[38] Saldin E.L. et al., Longitudinal Space Charge Driven Microbunching Instability in TTF2 Linac, TESAL-FEL-2003-02.
[39] Huang Z. et al., SLAC-PUB-10334, 2004.
[40] Lipka D, The use of the Streak Camera, PITZ note, 2003.
[41] Wu Juhao et al., SLAC-PUB-10430, 2004.
[42] Floettmann K., ASTRA User Manual http://www.desy.de/~mpyflo/Astra_dokumentation/
[43] Floettmann K., Phys. Rev. ST Accel. Beams 6, 034202 (2003).
[44] Mallat S., A Wavelet Tour of Signal Processing, Academic Press, 2001.
[45] Wong T. et al., Sampling with Hammersley and Halton Points, J. Graphics Tools, vol.2, no.2, 1997, pp.9-24.
[46] Jenkins G.M. and et al., Spectral Analysis and its Applications, Holden-Dan, 1969
[47] Vitiazev V.V., Wavelet analysis of time-series, St.Petersburg State University Publishing House, 2001 (in russian).